

# Reduced-Complexity

## Model Selection and Rate Allocation

### for Multiple-Model Electrical Signal Compression

Corentin Presvôts, Michel Kieffer, *Senior Member, IEEE*, Thibault Prevost

#### Abstract

This paper adapts a Multiple-Model Coding (MMC) approach for sampled electrical signal waveforms to satisfy reconstructed signal quality constraints. The baseline MMC approach consists of two stages processing vectors of Voltage and Current Signal (VCS) of constant size and producing bitstreams of constant rate but varying quality. In the proposed approach, the parametric model and the rate allocated to the first stage, as well as the residual compression method of the second stage and its associated rate, are jointly optimized to achieve a target distortion of the reconstructed signal. Three approaches are proposed. An exhaustive search serves as a baseline for comparison. Then, an approach involving a Golden Section search is exploited to determine the rate of the first stage with reduced complexity. Finally, rate-distortion models of the compression efficiency for each model in the first stage are employed to obtain a subset of promising models in the first stage and reduced-size search intervals for the rate selection in both stages. Simulation results demonstrate that the proposed reduced-complexity MMC approach reduces the rate for a given distortion constraint compared to state-of-the-art solutions for VCS with equivalent complexity.

#### Index Terms

Compression, low latency, model-based coding, rate-distortion optimization, electrical waveform compression

#### I. INTRODUCTION

Integrating renewable energy sources within the electrical grid introduces complex grid dynamics, as highlighted by [1]. A more efficient, reduced-latency control of the grid may be necessary. Such control requires transmitting large volumes of data from substations to higher-level control centers. To meet the rate constraints of communication networks, it is essential to develop efficient compression techniques tailored to the specific characteristics of electrical signals. Currently, Phasor Measurement Units (PMUs) are the most commonly deployed devices for acquiring and compressing electrical signals. PMUs, however, are unable to represent rapid transients accurately. VCS are better suited to detect and localize faults in the network or reduced-latency control tasks. Several techniques have been developed to compress VCS, as discussed in Section II.

This work extends the approach in [2], which introduced a two-stage MMC method for VCS. In the first stage, several parametric models are compared to obtain a coarse, low-bit-rate representation of the samples. In the second stage, various residual compression techniques are evaluated to minimize distortion. The selection of the optimal model in the first stage and the residual compression technique in the second stage, as well as the bit allocation between the two stages, are optimized considering a total bit budget constraint. This optimization may be complex and incompatible with real-time constraints. Moreover, imposing a bit budget constraint leads to variations in the reconstruction quality of the VCS.

This paper aims at determining the minimum total bit budget required to satisfy some maximum distortion constraint when VCS are compressed with the MMC approach in [2]. This approach ensures a target reconstruction quality, but requires a proper adaptation of the bit budget for each encoded group of the VCS, which increases the complexity of the MMC approach compared to the fixed-rate variant. Three methods are proposed. The first method involves an Exhaustive Search (ES) within some progressively refined interval to determine the bit allocation for the first stage. The second method involves the Golden Section Search (GSS) within the search interval. Finally, the third method leverages Rate-Distortion (RD) models to get an initial estimate of the bit allocation between the two stages for each considered model and to select a subset of promising candidate models and reduced-size search intervals for the rate. The optimal allocation between stages is then determined by applying one of the first two methods.

The remainder of this paper is organized as follows. Section II reviews some related work. Section III briefly summarizes the MMC approach of [2] and introduces the problem of optimizing the total bit budget, the model in the first stage, the compression method in the second stage, and the bit allocation between the two stages to meet some maximum distortion constraint. The methods for solving this problem are discussed in Section IV. Section V discusses a solution using RD models. Simulation results are presented in Section VI. Section VII concludes this paper.

## II. RELATED WORK

In lossy data compression, a compromise has to be found between the rate at which data are encoded, *i.e.*, the number of bits used to represent the compressed data, and the distortion of the reconstructed version of the data. Section II-A briefly recalls the methods used in image and video compression to reach a target rate-distortion compromise. Then, Section II-B recalls techniques for compressing electrical signals, some focusing on a target rate, others on a target distortion. Finally, Section II-C presents various two-stage compression methods, where an initial coarse compression is refined in a second stage to improve the rate-distortion balance. These methods involve higher computational costs, particularly to adjust the bit allocation between the two stages while satisfying a target rate or distortion constraint. This section also explores strategies proposed in the literature to balance computational complexity with rate or distortion objectives.

### A. Satisfying a rate or a distortion constraint in image or video coding

In real-time streaming, particularly over wireless networks, the available bandwidth is often constrained and time varying. Encoding Rate Control (RC) methods are then employed to adjust the compression rate to minimize distortion and avoid receiver buffer depletion. This is typically done by tuning the value of the Quantization Parameters (QPs) employed after transform coding of the prediction residuals. Instead of testing all combinations of QPs, rate and distortion models are exploited to evaluate the trade-off between rate and distortion as a function of characteristics of the encoded stream or of the coding parameters, such as the QPs.

Rate and distortion models fall into two broad categories: those assuming that data blocks serving as the basis for the compression process such as frames or Coding Units (CU) are independent, and those accounting for inter-dependencies.

For the first category, R-QP models predict the rate as a function of the quantization parameter QP by estimating the distortion between a coding unit and its predicted version, which allows the model to adapt the predicted rate according to the signal content. Commonly-used distortion metrics include the Mean Absolute Difference (MAD) [3], [4], the Sum of Absolute Difference (SAD) [5], [6], and the Mean Square Error (MSE) [7].. With R- $\rho$  models [8], the rate is predicted based on the percentage of zero-valued transformed coefficients. Finally, R- $\lambda$  models use a Lagrangian multiplier  $\lambda$  to control the rate-distortion trade-off [9]. A parametric R-D model is fitted from videos encoded at different QPs, and  $\lambda$  is defined as the negative slope of the R-D curve. The corresponding QP for a given  $\lambda$  approximately minimizes  $D + \lambda R$ , achieving the desired balance between rate and distortion. Experiments in [10], [11] show that R- $\lambda$ -based rate control algorithms outperform those based on R-QP or R- $\rho$  models.

In the second category, methods like those in [9], [12] predict the rate using the standard deviation of motion-compensated residuals. Unlike R- $\rho$  models, where MAD, SAD, or MSE are computed solely from the local characteristics of a CU, these models account for the propagation between blocks of the prediction errors. Other approaches use cubic models [13], [14] to predict the rate based on the values of QP of both the current and reference frames. In [7], an R-D-QP model is considered where the rate is predicted as a function of the distortion of the reference frame and the average QP of the current frame. Deep learning-based methods are also used to estimate the reconstruction quality at a given rate using previous images and the current image, allowing the frame reconstruction quality to be adjusted via QP [15], [16].

Scalable coders generate a single bitstream from which reconstructions with different quality levels are obtained, depending on the proportion of bits taken from the bitstream [17], [18]. Coarse-Grain Scalability (CGS) [19], [20] refines the prediction residuals in discrete steps or layers, each providing an improvement in quality. Fine Grain Scalability (FGS) [21] progressively refines the prediction residuals with finer increments, allowing for a more flexible adjustment of quality based on the available rate. Historical

examples of scalable coding methods dedicated to image coding are Embedded Zerotree Wavelet (EZW) [22], Layered Zero Coding (LZC) [23], Set Partitioning in Hierarchical Trees (SPIHT) [24], or Embedded Block Coding with Optimized Truncation of the embedded bit-streams (EBCOT) [25]. Recent scalable extensions of video coders are Scalable High Efficiency Video Coding (SHEVC) [26], Scalable Video Technology (SVT) for AOMedia Video 1 (AV1) [27], or the Low Complexity Enhancement Video Coding (LCEVC) [28]. Nevertheless, generating a scalable bitstream usually results in some loss in compression performance compared to a non-scalable approach tuned using an R-D model [17].

In recently-developed neural compression approaches [29]–[33], a trainable autoencoder architecture is optimized by taking into account both quantization and entropy coding. The loss function is the rate-distortion trade-off  $R + \lambda D$  for a given regularization parameter  $\lambda$ , but there is no strict constraint on the rate or distortion and several pre-trained models for different values of  $\lambda$  are required to handle different target rates. To address this issue, coarse-grain scalable learning-based coding schemes have been proposed [34]–[36]. A base-resolution layer provides a coarse reconstruction of the data, followed by several enhancement layers. To reduce the correlation between layers, each enhancement layer predicts the residuals during training.

### *B. Baseline approaches for rate or distortion constraint satisfaction in electrical signal compression*

1) *Parametric coding*: Parametric coding approaches represent signals with one or few parametric models including sum of sinusoids or damped sinusoids [37]–[43] to exploit the physical properties of signals to compress. Phasor Measurement Units (PMUs) use a sinusoidal model characterized by its amplitude, frequency, and phase. In the standard [44], each of these three parameters is encoded using 12 bytes. Depending on the acquisition frequency, the volume of data generated can be large. For example, one PMUs collecting 20 measurements at 30 Hz sampling rate generates over 500 MBytes of data per day [45].

The compression approaches for non-stationary signals in power systems have recently shifted from traditional phasor-based approaches towards methods that leverage more sophisticated parametric models. The classic stationary phasor representation is often insufficient to capture the broadband dynamics induced by modern grid conditions, such as frequency ramps, amplitude modulations, and step changes in renewable-dominated networks [46].

The sinusoidal model used in the PMUs has been extended by decomposing the signal into a sum of parametric damped sinusoids [47], [48] each of which is represented by four parameters: amplitude, frequency, phase, and damping factor. Similarly, [49], [50] decomposes the signal into a sum of piecewise damped sinusoids, requiring two additional parameters per model to define the window size for each damped sinusoid. In [51], [52], the signal is also decomposed as a sum of damped sinusoids, gathered in a parametric dictionary. The minimum number of dictionary elements (atoms) is selected so as to satisfy a reconstruction quality constraint. The atom parameters are quantized with several quantizers, each of

which defines a dictionary of quantized parameters. Therefore, testing different quantizers is equivalent to testing different dictionaries. For every candidate dictionary, the rate–distortion trade-off is evaluated, and the one that minimizes bitrate while respecting the distortion constraint is selected.

Extending these ideas, [53], [54] introduce a dictionary-based approach that uses a set of predefined parametric models such as amplitude modulations, frequency ramps, phase modulations, amplitude steps, and phase steps, to model typical grid disturbances. In [55], the dictionary is iteratively constructed using equiangular tight frames with minimal coherence to enhance signal representation and separation. Nevertheless, no explicit quantization or entropy coding is applied. Compression is achieved by retaining only a small subset of dictionary elements to represent the original signal.

2) *Transform coding*: Transform coding is a widely-used technique for signal compression, able to capture the transient nature of signals. Among the various transforms, the Discrete Cosine Transform (DCT) [56], [57], the Fourier transform [58], [59], and the Discrete Wavelet Transform (DWT) [60]–[67] have been mainly exploited. Other transforms include the Slantlet transform [68], spline wavelets [69], [70], wavelet packet-enhanced transforms [71], [72], the Hartley transform [56], [73], filter banks [74], or trainable transforms [29]–[33] adapted for electrical signal compression [2], [75].

After the signal transform, only the most significant coefficients are kept [56], [60], [62], [76]. Their number is determined by a rate or distortion constraint. The position (index) and amplitude of the coefficients have to be transmitted to the decoder for signal reconstruction. In [56], significant coefficients are iteratively selected until a distortion criterion is met. The positions of these coefficients are encoded via run-length coding, while their amplitudes are mapped to a codebook optimized using the Linde–Buzo–Gray algorithm [77]. In [60], [62], only the most significant wavelet coefficients are retained and entropy-coded via Lempel Ziv Welch (LZW) in [60] or Huffman coding in [62]. In [76], the most significant coefficients are determined using the Minimum Description Length (MDL) criterion [78], which allows the selection of significant coefficients by minimizing a rate-distortion compromise. The amplitudes and positions are then encoded using LZW or Huffman coding. These approaches thus easily achieve rate or distortion constraints within a margin corresponding to the rate required to represent one significant coefficient. In [64], [66], [67], [79], a threshold (to zero out insignificant coefficients) and the QP are adjusted to meet a rate or distortion constraint.

In [63], [65], vector quantization is employed. The quantization cells are trained using a set of representative test signals. The coefficients are then mapped to a pre-trained codebook. The rate or distortion is adjusted by controlling the codebook size or selecting different quantization levels for the coefficients. More recently, in [59], significant coefficients are selected based on a threshold derived from the minimum, maximum, and mean values of the transformed coefficients, and the retained coefficients, along with their positions, are encoded using a lossless method like LZW coding.

To optimize the quantization of transformed coefficients, [58], [73], [80], [81] exploit linear [80] or polynomial [58] models approximating the envelope of the spectral coefficients to capture the global

energy distribution across frequencies. These models yield a prediction of the amplitude of coefficients in different bands, facilitating adaptive quantization. In [80], a non-parametric model is considered based on spectral estimation from a set of dictionaries whose components represent the spectral signature of power system disturbances. Dynamic spectral prediction models are introduced in [73], [81], based either on the variance of the coefficients or on their maximum value.

Inspired by image compression, scalable compression schemes, such as the EZW bit-plane coding method, have been adapted to one-dimensional signals in [61], [82]. In [83] as in [2], [75], DCT is followed by bit-plane coding. Variational autoencoders have been applied in [2], [75], trained on disturbance signals [84] to optimize the end-to-end compression pipeline. Nevertheless, the rate-distortion compromise is adjusted during training and cannot be perfectly met for specific signals.

3) *Dictionary coding*: Dictionary coding approaches decompose the signal to compress into a linear combination of vectors from a predefined dictionary of signals. For example, in [85], [86], the dictionaries consist of cosines, sines, and Dirac functions which, compared to DCT or DWT, yield a better representation of signals with localized defects. The dictionary consists of damped sinusoids, cosines, and Gabor functions in [87] and of cosines and wavelets in [88]. The combination of these functions provides higher levels of sparsity compared to [50], [85], at the price of an increased computational complexity.

Matching pursuit algorithms [89] are commonly used to select the combination of dictionary elements representing the signal. The encoding process stops once the required number of selected elements is reached, making it easier to meet either rate or distortion constraints. In [87] artificial neural network select the best sub-dictionary used at each matching pursuit iteration.

### *C. Rate and distortion optimization in two-stage schemes*

In two-stage compression approaches such as [90]–[92], considering a total bit budget, the first stage performs parametric coding of the main signal components, while the second stage encodes the residual using a transform-based method. One of the difficulties is to determine the bit allocation between stages to maximize the reconstruction quality. In [90]–[92], a fixed number of bits is used in the first stage to represent sinusoidal components, producing a coarse reconstruction. The residual is then encoded using a non-parametric approach to reach the target distortion. In [93], the signal is decomposed into a sum of damped sinusoids until a first distortion target is reached. The reconstruction residual from the first stage is encoded using a DWT followed by entropy coding until the final distortion target is attained. Nevertheless, imposing a fixed rate or distortion target in the first stage is not necessarily optimal: the efficiency of the first stage is often dependent on the signal characteristics. In [75], the rate allocation between the two stages is optimized to get the minimum distortion. Nevertheless, this approach is computationally demanding, since for each choice of the rate allocation in the first stage, a different residual is obtained with a different rate-distortion characteristic. Moreover, no distortion target satisfaction is considered.

### III. PROBLEM FORMULATION

This section briefly recalls the two-stage multiple-model electrical signal compression approach introduced in [75]. Then, the problem of minimizing the total bit budget under a target distortion constraint is formulated. This problem involves the joint selection of (i) the model in the first stage, (ii) the bit budget to encode its estimated parameters, (iii) the bit allocation among the components of the parameter vector, (iv) the residual compression method, and (v) the bit budget in the second stage.

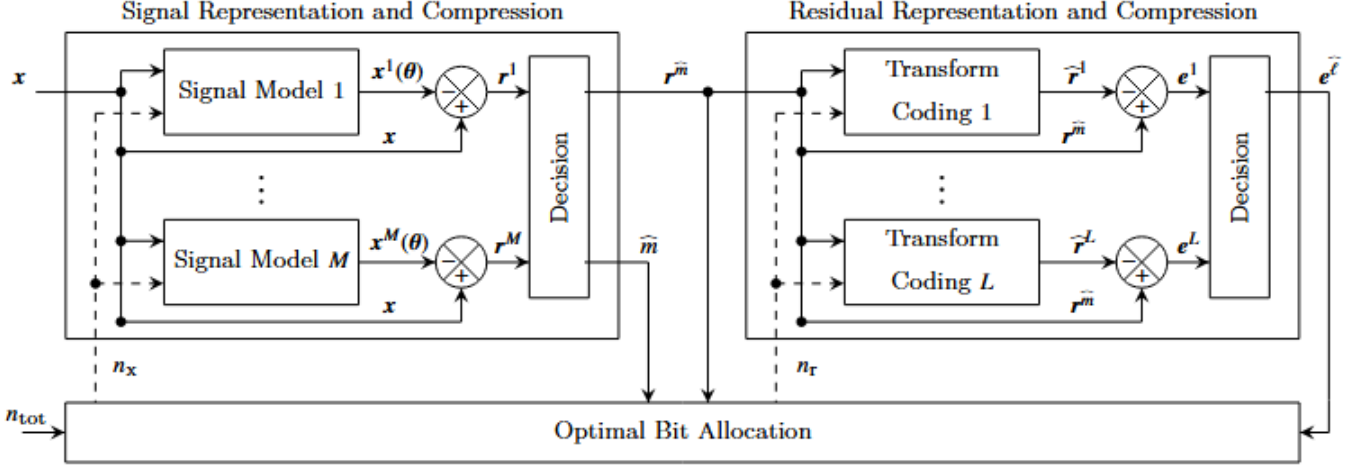


Fig. 1. Diagram of the two-stage multiple-model electrical signal compression approach introduced in [75].

#### A. Two-stage multiple-model electrical signal compression approach

Consider an alternating single-phase signal  $x(t)$  acquired within an electrical substation at a sampling period  $T_s = 1/f_s$ . The sample of  $x(t)$  at time  $kT_s$ ,  $k \in \mathbb{Z}$ , is denoted  $x_k$ . Vectors of  $N$  consecutive samples  $\mathbf{x}_i = (x_{iN+1}, \dots, x_{(i+1)N})^T$ ,  $i \in \mathbb{Z}$ , are compressed immediately after their acquisition. The reconstructed vector is denoted  $\hat{\mathbf{x}}_i = (\hat{x}_{iN+1}, \dots, \hat{x}_{(i+1)N})^T$ ,  $i \in \mathbb{Z}$ . The aim is to design a coding scheme that minimizes the MSE between  $\mathbf{x}_i$  and  $\hat{\mathbf{x}}_i$ . Without loss of generality, we consider the compression of  $\mathbf{x}_0 = (x_1, \dots, x_N)^T$ . Moreover, to further lighten notations, when  $\mathbf{x}_0$  is processed independently of the previous vectors, the subscript 0 is omitted.

The compression of  $\mathbf{x}$  is performed in two stages, presented in Figure 1. In the first stage,  $M$  parametric models with output  $\mathbf{x}^m(\boldsymbol{\theta})$ ,  $m \in \mathcal{M} = \{1, \dots, M\}$ , are put in competition. The vector  $\boldsymbol{\theta} \in \mathbb{R}^{K^m}$  of  $K^m$  parameters of the  $m$ -th model is assumed to follow an *a priori* distribution  $p^m(\boldsymbol{\theta})$ , specified in the model. For the  $m$ -th model, the estimate of  $\boldsymbol{\theta}$  minimizing the norm of the estimation residual  $\mathbf{r}^m(\boldsymbol{\theta}) = \mathbf{x} - \mathbf{x}^m(\boldsymbol{\theta})$  is

$$\hat{\boldsymbol{\theta}} = \arg \min_{\boldsymbol{\theta}} \frac{1}{N} \|\mathbf{r}^m(\boldsymbol{\theta})\|^2. \quad (1)$$

The estimate  $\hat{\boldsymbol{\theta}}$  is quantized and represented using a budget of  $n_x$  bits to get  $\hat{\boldsymbol{\theta}}_q(n_x)$ . The dependency of quantized vectors in the bit budget is often omitted in what follows. The selected model  $\hat{m}$  is the one

minimizing the norm of the estimation residual  $\mathbf{r}^m(\hat{\boldsymbol{\theta}}_q)$ , evaluated considering the quantized version of the estimated parameter vector. A coarse representation  $\mathbf{x}^{\hat{m}}(\hat{\boldsymbol{\theta}}_q)$  of  $\mathbf{x}$  is then obtained at the output at the first stage, as well as  $\mathbf{r}^{\hat{m}}(\hat{\boldsymbol{\theta}}_q)$ , to be processed by the second stage.

Many models can be considered in the first stage, such as the sinusoidal model

$$x_n(\boldsymbol{\theta}) = a \cos(2\pi f n T_s + \phi), \quad n = 1, \dots, N, \quad (2)$$

with  $\boldsymbol{\theta} = (a, f, \phi)^T$  or linear combinations of  $K$  Tchebychev polynomials of the first kind  $\mathcal{T}_k$  of degree  $k$  [94], with output

$$x_n(\boldsymbol{\theta}) = \sum_{k=0}^{K-1} \theta_{k+1} \mathcal{T}_k\left(2 \frac{n}{N} - 1\right), \quad n = 1, \dots, N, \quad (3)$$

and vector of parameters  $\boldsymbol{\theta} = (\theta_1, \dots, \theta_K)^T$ . Additional sample predictive and parameter predictive models have been considered in [2], [75] to represent the samples of  $\mathbf{x}_i$  using previously encoded samples or previously considered models. In the sample predictive model, a model of  $\mathbf{x}_i$  is built using the reconstructed samples  $\hat{x}_{iN}, \hat{x}_{iN-1} \dots$  considering a linear predictor of order  $K$ , offset  $\eta \geq 0$ , and gains  $\theta_1, \dots, \theta_K$  as

$$x_n(\boldsymbol{\theta}) = \sum_{k=1}^K \theta_k \hat{x}_{(i-1)N+n-\eta-k+1}, \quad n = 1, \dots, N, \quad (4)$$

and  $\boldsymbol{\theta} = (\theta_1, \dots, \theta_K)^T$ . In the parameter predictive model, to represent  $\mathbf{x}_i$ , the model of index  $\hat{m}_{i-1}$  and quantized parameter vector  $\hat{\boldsymbol{\theta}}_{i-1,q}$  is reused and a differential coding of the vector of parameters is performed by evaluating

$$\hat{\boldsymbol{\delta}} = \arg \min_{\boldsymbol{\delta}} \frac{1}{N} \left\| \mathbf{x}_i - \mathbf{x}^{\hat{m}_{i-1}} \left( \hat{\boldsymbol{\theta}}_{i-1,q} + \boldsymbol{\delta} \right) \right\|^2. \quad (5)$$

Then  $\hat{\boldsymbol{\delta}}$  is quantized and represented using a budget of  $n_x$  bits to get  $\hat{\boldsymbol{\delta}}_q$ . The model output is obtained using (2), (3), or (4) with  $\hat{\boldsymbol{\theta}}_{i,q} = \hat{\boldsymbol{\theta}}_{i-1,q} + \hat{\boldsymbol{\delta}}_q$ . Finally, the option of bypassing the first stage is considered when no parametric model can adequately represent the original signal. In this case, a null model with output

$$x_n(\boldsymbol{\theta}) = 0, \quad n = 1, \dots, N, \quad (6)$$

is employed, with  $\boldsymbol{\theta} = \emptyset$ .

In the second stage,  $L$  residual compression methods are compared, each of which providing an estimate  $\hat{\mathbf{r}}^\ell$  of  $\mathbf{r}^{\hat{m}}(\hat{\boldsymbol{\theta}}_q)$ . The method  $\hat{\ell}$  that yields the smallest norm of the residual  $\mathbf{e}^\ell = \mathbf{r}^{\hat{m}}(\hat{\boldsymbol{\theta}}_q) - \hat{\mathbf{r}}^\ell$  for a given bit budget  $n_r$  is selected. In addition to DCT and DWT, trainable transforms based on Variational Auto Encoder (VAE) [30], [32], [95] are also considered. The second stage may also be bypassed when the first stage represents efficiently enough the signal  $\mathbf{x}$  (when the distortion target is met).

Among the  $n_{\text{tot}}$  bits available to represent  $\mathbf{x}$ ,  $n_x$  are used for the quantized model parameter vector,  $n_r$  for the residual, and  $n_h$  for all additional (header) information required to reconstruct  $\mathbf{x}$ . The allocation of  $n_{\text{tot}}$  among  $n_h$ ,  $n_x$ , and  $n_r$  has thus to be optimized.

The dynamic range of signals and residuals may vary significantly. To address this issue,  $\mathbf{x}$  (before the first stage) and  $\mathbf{r}^{\hat{m}}(\hat{\boldsymbol{\theta}}_q)$  (before the second stage) are multiplied by  $2^{k_x}$  and  $2^{k_r}$  respectively, where the scaling coefficients  $k_x \in \mathbb{Z}$  and  $k_r \in \mathbb{Z}$  are such that  $\max(2^{k_x} |\mathbf{x}|) \in [0.5, 1[$  and  $\max(2^{k_r} |\mathbf{r}^{\hat{m}}(\hat{\boldsymbol{\theta}}_q)|) \in [0.5, 1[$ . The parameters  $k_x$  and  $k_r$  are stored in the header, with a fixed-length representation, using part of the  $n_h$  bits.

### B. Optimization of the compression parameters under a distortion constraint

For a given vector  $\mathbf{x}$ , consider the first-stage model output  $\mathbf{x}^m(\hat{\boldsymbol{\theta}}_q(n_x))$  where  $\hat{\boldsymbol{\theta}}$  has been represented with  $n_x$  bits and the second-stage reconstructed residual  $\hat{\mathbf{r}}^\ell(n_r)$  with a bit budget  $n_r$ . To recover an estimate of the original vector from the output of both stages,  $n_h$  bits are required to represent  $n_x$  and  $n_r$  themselves, the scaling factors  $k_x$  and  $k_r$ , and the indices of the best model  $\hat{m}$  and the best compression method  $\hat{\ell}$ . We assume that  $m$ ,  $\ell$ ,  $k_x$ ,  $k_r$ ,  $n_x$ , and  $n_r$  are represented with a fixed-length code in the header and that  $n_h$  is therefore constant.

Our aim in what follows is, considering some target distortion constraint  $D_{\max}$ , to determine the optimal values of  $m$ ,  $\ell$ ,  $n_x$ , and  $n_r$ , which are the solution of the following constrained optimization problem

$$\begin{aligned} \hat{m}, \hat{\ell}, \hat{n}_x, \hat{n}_r &= \arg \min_{m, \ell, n_x, n_r} n_h + n_x + n_r \\ \text{s.t. } D^{m, \ell}(n_x, n_r) &\leq D_{\max}. \end{aligned} \quad (7)$$

where

$$D^{m, \ell}(n_x, n_r) = \frac{1}{N} \left\| \mathbf{x} - \mathbf{x}^m(\hat{\boldsymbol{\theta}}_q(n_x)) - \hat{\mathbf{r}}^\ell(n_r) \right\|^2 \quad (8)$$

is the distortion obtained at the output of the second stage, when the  $m$ -th model is used with parameter vector  $\hat{\boldsymbol{\theta}}$  quantized with  $n_x$  bits and when the  $\ell$ -th residual compression method is used with  $n_r$  bits.

## IV. PROPOSED SOLUTIONS

To address the optimization problem in (7), Section IV-A first describes, for a given value of  $n_x$ , the allocation of these bits across components of the quantized model parameter vector. Since the value of  $n_x$ , solution of (7), is not known *a priori*, Section IV-B determines a search interval for candidate values of  $n_x$  so as to reduce the number of cases to consider. Section IV-C details an ES method to identify the allocation of  $n_x$  and  $n_r$ , achieving an optimal solution for (7). Finally, Section IV-D describes a reduced-complexity approach based on GSS.

### A. Representation of the Quantized Model Parameters

In the first compression stage, consider the  $m$ -th model and a budget of  $n_x$  bits to represent the vector of parameters  $\hat{\boldsymbol{\theta}}$ . In this paper, a scalar quantization of each component of  $\hat{\boldsymbol{\theta}}$  is performed to get

$\widehat{\boldsymbol{\theta}}_q(n_1, \dots, n_K)$ , where  $n_k$  is the number of bits used to represent the  $k$ -th parameter  $\widehat{\theta}_k$ . The quantization of  $\widehat{\boldsymbol{\theta}}$  introduces an error in the model output expressed as

$$\boldsymbol{\varepsilon}_q^m(\widehat{\boldsymbol{\theta}}, (n_1, \dots, n_K)) = \mathbf{x}^m(\widehat{\boldsymbol{\theta}}) - \mathbf{x}^m(\widehat{\boldsymbol{\theta}}_q(n_1, \dots, n_K)). \quad (9)$$

Our aim is to determine the allocation of bits  $n_k$ ,  $k = 1, \dots, K$ , that minimizes the expected norm of the error introduced by the quantization of  $\widehat{\boldsymbol{\theta}}$  on the model output

$$\begin{aligned} \widehat{n}_1, \dots, \widehat{n}_K &= \arg \min_{n_1, \dots, n_K} \mathbb{E}_{\widehat{\boldsymbol{\theta}}} \left[ \frac{1}{N} \left\| \mathbf{x}^m(\widehat{\boldsymbol{\theta}}) - \mathbf{x}^m(\widehat{\boldsymbol{\theta}}_q(n_1, \dots, n_K)) \right\|^2 \right] \\ \text{s.t. } & \sum_{k=1}^K n_k = n_x, \end{aligned} \quad (10)$$

where the expectations is evaluated with respect to the *a priori* distribution of  $\widehat{\boldsymbol{\theta}}$ . The aim is to get values  $\widehat{n}_k$  for  $k = 1, \dots, K$  that are independent of the signal samples to be encoded and are only characteristics of the model  $m$  for a given  $n_x$ . This avoids transmitting  $\widehat{n}_k$ , for  $k = 1, \dots, K$ , provided that an offline optimization has been done for a sufficiently large variety of values of  $n_x$ .

Proposition 1 provides an approximate expression of the expected value of the norm of the error induced by the quantization of  $\widehat{\boldsymbol{\theta}}$ .

**Proposition 1.** *Assuming that the components of the quantization error  $\boldsymbol{\varepsilon} = \widehat{\boldsymbol{\theta}} - \widehat{\boldsymbol{\theta}}_q$  of the parameter vector  $\widehat{\boldsymbol{\theta}}$  are zero-mean and uncorrelated and that they are uncorrelated with  $\frac{\partial \mathbf{x}_n^m(\boldsymbol{\theta})}{\partial \theta_k}$  for all  $k = 1, \dots, K$  and  $n = 1, \dots, N$ , one has*

$$\mathbb{E}_{\widehat{\boldsymbol{\theta}}} \left[ \frac{1}{N} \left\| \mathbf{x}^m(\widehat{\boldsymbol{\theta}}) - \mathbf{x}^m(\widehat{\boldsymbol{\theta}}_q(n_1, \dots, n_K)) \right\|^2 \right] = \sum_{k=1}^K h_k \mathbb{E}_{\widehat{\theta}_k} [\varepsilon_k^2], \quad (11)$$

where  $\varepsilon_k$  is the  $k$ -th component of  $\boldsymbol{\varepsilon}$  and

$$h_k = \mathbb{E}_{\widehat{\boldsymbol{\theta}}} \left[ \frac{1}{N} \left\| \frac{\partial \mathbf{x}^m(\boldsymbol{\theta})}{\partial \theta_k} \right\|^2 \right]. \quad (12)$$

*Proof.* Proposition 1 is a special case of Proposition 3, which proof is in Appendix A.  $\square$

The components  $h_k$  introduced in (12) are the expected values of the squared norm of the sensitivity of  $\mathbf{x}^m(\boldsymbol{\theta})$  with respect to  $\theta_k$  and depend on the chosen model. It has been shown in [75] that for a sinusoidal model,  $h_1 = 1/2$ ,  $h_2 = \mathbb{E}[a^2] (2\pi N T_s)^2 / 6$ , and  $h_3 = \mathbb{E}[a^2] / 2$ . For a Tchebychev polynomial model of degree  $k$ ,  $h_k = \frac{1}{N} \sum_{n=1}^N \mathcal{T}_k^2(2n/N - 1)$ ,  $k = 0, \dots, K-1$ . For a sample predictive model of order  $k$  and offset  $\eta$ ,  $h_k = \frac{1}{N} \sum_{n=1}^N \widehat{x}_{(i-1)N+n-\eta-k+1}^2$ ,  $k = 1, \dots, K$ . For parameter predictive model, the entries of  $\widehat{\boldsymbol{\delta}}$  are scalar quantized to get  $\widehat{\boldsymbol{\delta}}_q = \widehat{\boldsymbol{\delta}} + \boldsymbol{\varepsilon}$ , where  $\boldsymbol{\varepsilon}$  is the quantization error vector. Consequently, the optimal bit allocation for the quantization can be done considering  $\widehat{\boldsymbol{\delta}}$  instead of  $\widehat{\boldsymbol{\theta}}$ , whatever the model.

Assuming a smooth distribution  $p(\widehat{\boldsymbol{\theta}})$ , at high rate one gets  $\mathbb{E}_{\widehat{\boldsymbol{\theta}}} [\varepsilon_k^2] = c_k^2 2^{-2n_k}$  [96], with

$$c_k^2 = \frac{1}{12} \left[ \int_{\mathbb{R}} \sqrt[3]{p(\widehat{\theta}_k)} d\widehat{\theta}_k \right]^3. \quad (13)$$

For example, if  $\widehat{\theta}_k$  is uniformly distributed over an interval of width  $w_k$ , then  $c_k^2 = \frac{w_k^2}{12}$ . If  $\widehat{\theta}_k$  follows a Gaussian distribution of variance  $\sigma_k^2$ , then  $c_k^2 = \frac{\sqrt{3}\pi}{2}\sigma_k^2$ .

**Proposition 2.** Consider a model with  $K$  parameters. Assume that the  $k$ -th parameter is scalar quantized with  $n_k$  bits and that  $\mathbb{E}_{\widehat{\theta}_k} \left[ \left( \widehat{\theta}_k - \widehat{\theta}_{q,k} \right)^2 \right] = c_k^2 2^{-2n_k}$  for some  $c_k$ . Assume without loss of generality that  $p_1 c_1^2 \geq \dots \geq h_K c_K^2$ . Then, the solution of (10) is

$$\widehat{n}_k = \frac{n_x}{K'} + \frac{1}{2} \log_2 \frac{h_k c_k^2}{\left( \prod_{j=1}^{K'} h_j c_j^2 \right)^{1/K'}}, \quad k = 1, \dots, K', \quad (14)$$

$$\widehat{n}_k = 0, \quad k = K' + 1, \dots, K, \quad (15)$$

where  $K' \leq K$  is the largest integer such that  $\widehat{n}_k \geq 0$ ,  $k = 1, \dots, K'$ .

*Proof.* The proof is similar to that for the bit allocation for independent Gaussian sources minimizing the total quadratic distortion, where the variance of the sources is replaced by  $h_k c_k^2$ , see [97, Chap.13.5].  $\square$

The expression (14) takes into account the sensitivity of the model with respect to its parameters. More rate is allocated to parameters for which the term  $h_k c_k^2$  is larger than the geometric mean of the  $K'$  largest terms.

In what follows,  $\varepsilon_q^m(\widehat{\theta}, n_x)$  represents the vector  $\varepsilon_q^m(\widehat{\theta}, (\widehat{n}_1, \dots, \widehat{n}_K))$ , with  $\widehat{n}_1, \dots, \widehat{n}_K$  obtained from Proposition 2.

### B. Search Interval for $n_x$

An upper bound  $n_{\max}$  for the number of bits  $n_x$  to use in the first stage can be obtained by evaluating the rate that would be required by the second stage to meet the target distortion when skipping the first stage. In such case,  $\mathbf{x}$  is directly represented by  $\widehat{\mathbf{r}}^\ell(n)$  and for the  $\ell$ -th residual compression method, one has

$$n_{\max}^\ell = \min n \quad \text{s.t.} \quad \frac{1}{N} \left\| \mathbf{x} - \widehat{\mathbf{r}}^\ell(n) \right\|^2 \leq D_{\max}, \quad (16)$$

$$n_{\max} = \min_\ell n_{\max}^\ell \quad (17)$$

and

$$\underline{\ell} = \arg \min_\ell n_{\max}^\ell. \quad (18)$$

Now, consider the model  $m$  in the first stage. If the quantization error of the estimated parameter vector  $\widehat{\theta}$  is neglected, the rate required by the second stage to represent the residual  $\mathbf{x} - \mathbf{x}^m(\widehat{\theta})$  with the target distortion would be

$$n_{\min}^m = \min_\ell n_{\min}^{m,\ell}, \quad (19)$$

where

$$n_{\min}^{m,\ell} = \min n \quad \text{s.t.} \quad \frac{1}{N} \left\| \mathbf{x} - \mathbf{x}^m(\widehat{\theta}) - \widehat{\mathbf{r}}^\ell(n) \right\|^2 \leq D_{\max} \quad (20)$$

is the rate using the  $\ell$ -th compression method. In practice, the rate required by the second stage is in general larger than  $n_{\min}^{m,\ell}$ , to compensate the impact of the quantization error, since, according to (1), one has

$$\frac{1}{N} \left\| \mathbf{x} - \mathbf{x}^m(\widehat{\boldsymbol{\theta}}_q(n_x)) \right\|^2 \geq \frac{1}{N} \left\| \mathbf{x} - \mathbf{x}^m(\widehat{\boldsymbol{\theta}}) \right\|^2. \quad (21)$$

Moreover, considering  $n_x > n_{\max} - n_{\min}^m$  is useless as  $n_x + n_{\min}^m > n_{\max}$  bits would be required by the two stages, which is more than the amount  $n_{\max}$  of bits required considering only the second stage. Therefore, for a given model  $m$ , the search space for the number of bits  $n_x$  for the first stage can be reduced to the interval  $\mathcal{N}_x^m = [0, \dots, n_{\max} - n_{\min}^m]$ .

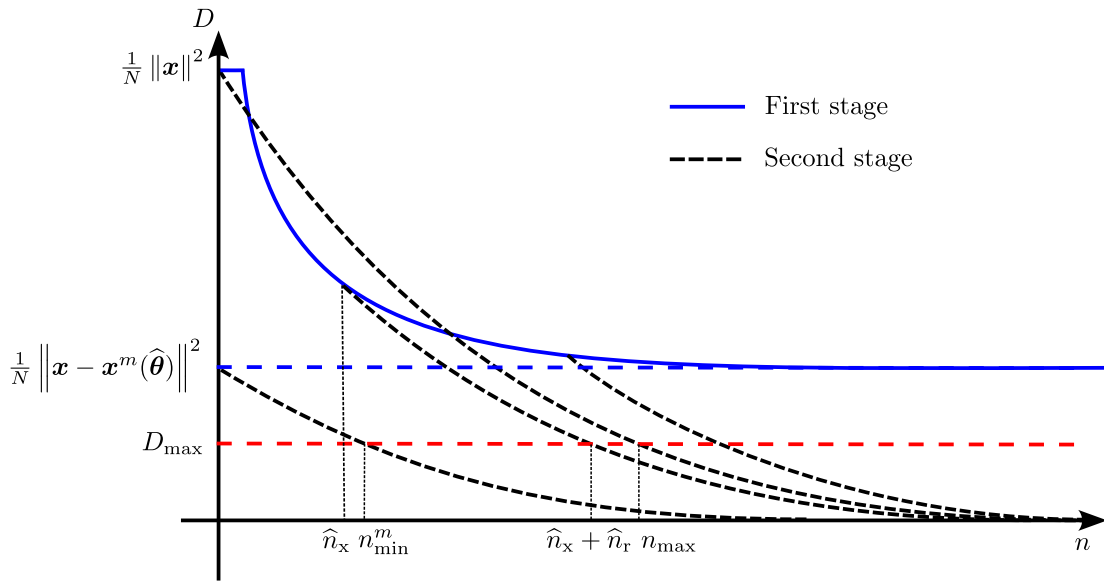


Fig. 2. Evolution of the distortion as a function of  $n_x$  for the first stage and  $n_x + n_r$  for the first and the second stages. The blue curve shows the distortion of the first stage as a function of  $n_x$ . The dotted black curves represent the residual distortion of the output of the second stage for different values of  $n_x$  and as a function of  $n_x + n_r$ . The black dashed curve starting at  $D = \frac{1}{N} \|\mathbf{x}\|^2$  represents the case where only the second stage is used. The point at which this curve intersects the red dashed line representing  $D_{\max}$  yields  $n_{\max}$ . The dotted black curve that begins at  $\frac{1}{N} \left\| \mathbf{x} - \mathbf{x}^m(\widehat{\boldsymbol{\theta}}) \right\|^2$  represents the residual distortion of the output of the second stage when the quantization error at the first stage is neglected ( $\widehat{\boldsymbol{\theta}}_q(n_x) = \widehat{\boldsymbol{\theta}}$ ). The minimum rate  $n_{\min}^m$  is determined at the intersection of this curve with  $D_{\max}$ . The two remaining black curves illustrate other scenarios for different values of  $n_x$ , demonstrating that the total number of bits required to satisfy the distortion constraint can vary depending on the choice of  $n_x$ .

Figure 2 illustrates the evolution of distortion as a function of  $n_x$  for the first stage (blue curve) and of  $n_x + n_r$  for the combined first and second stages (black dashed curves). The distortion at the output of the first stage when the  $m$ -th model is considered reaches the minimum  $\frac{1}{N} \left\| \mathbf{x} - \mathbf{x}^m(\widehat{\boldsymbol{\theta}}) \right\|^2$  corresponding to the absence of quantization of the estimated parameter vector  $\widehat{\boldsymbol{\theta}}$ . The dotted black curves represent the residual distortion at the output of the second stage for different values of  $n_x$  as a function of  $n_x + n_r$ . The black dashed curve starting at  $D = \frac{1}{N} \|\mathbf{x}\|^2$  represents the case where only the second stage is used. The point at which this curve intersects the red dashed line representing  $D_{\max}$  yields  $n_{\max}$ . The dotted black curve that begins at  $\frac{1}{N} \left\| \mathbf{x} - \mathbf{x}^m(\widehat{\boldsymbol{\theta}}) \right\|^2$  represents the residual distortion of the output of the second stage when the quantization error at the first stage is neglected ( $\widehat{\boldsymbol{\theta}}_q(n_x) = \widehat{\boldsymbol{\theta}}$ ). The minimum rate  $n_{\min}^m$  is determined at the intersection of this curve with  $D_{\max}$ . The two remaining black curves illustrate other scenarios for different values of  $n_x$ , demonstrating that the total number of bits required to satisfy the distortion constraint can vary depending on the choice of  $n_x$ .

### C. Exhaustive Search

In this section, the optimization problem (7) is solved via an ES, as detailed in Algorithm 1.

First, the upper bound  $n_{\max}$  is determined using (16) (line 1). For each model  $m \in \mathcal{M}$  (line 2),  $\widehat{\boldsymbol{\theta}}$  is estimated using (1) (line 3), and  $n_{\min}^m$  is evaluated using (20) (line 4). The set of candidate values  $\mathcal{N}_x^m$  for  $n_x$  is then obtained (line 5).

For each  $n_x \in \mathcal{N}_x^m$ ,  $\widehat{\boldsymbol{\theta}}$  is quantized to get  $\widehat{\boldsymbol{\theta}}_q(n_x)$  using the bit allocation from Proposition 2 (line 7). Then, for each residual compression method  $\ell \in \mathcal{L}$ , the distortion

$$D^{m,\ell}(n_x, n_r) = \frac{1}{N} \left\| \mathbf{x} - \mathbf{x}^m \left( \widehat{\boldsymbol{\theta}}_q(n_x) \right) - \widehat{\mathbf{r}}^\ell(n_r) \right\|^2 \quad (22)$$

is evaluated for increasing values of  $n_r$  (line 8) until the distortion constraint  $D_{\max}$  is satisfied for  $\underline{n}_r^\ell$ . Then,  $n_r(n_x)$ , the smallest value of  $\underline{n}_r^\ell$ ,  $\ell \in \mathcal{L}$  and the corresponding index of the second-stage compression approach  $\underline{\ell}$  are stored (line 11). If, for  $n_x$ , the model  $m$  is such that  $n_x + n_r(n_x) < n_{\max}$ , then  $n_{\max}$  and  $\mathcal{N}_x^m$  are updated (lines 13 and 14). Moreover, the values of  $n_x$ ,  $n_r$ , the corresponding model  $m$ , and residual compression method  $\ell$  are stored as candidate output of the algorithm (line 15).

---

#### Algorithm 1: Optimal solution for (7) via exhaustive search

---

```

1 Determine  $n_{\max}$  using (16);
2 for  $m \in \mathcal{M}$  do
3   Evaluate  $\widehat{\boldsymbol{\theta}}$  using (1) ;
4   Evaluate  $n_{\min}^m$  using (20) ;
5   Initialize  $\mathcal{N}_x^m = [0, n_{\max} - n_{\min}^m]$ ;
6   for each  $n_x \in \mathcal{N}_x^m$  do
7     Quantize  $\widehat{\boldsymbol{\theta}}$  to get  $\widehat{\boldsymbol{\theta}}_q(n_x)$  using the bit allocation of Proposition 2;
8     for each  $\ell \in \mathcal{L}$  do
9       Find  $\underline{n}_r^\ell$ , the smallest value of  $n_r^\ell$  such that  $\frac{1}{N} \left\| \mathbf{x} - \mathbf{x}^m \left( \widehat{\boldsymbol{\theta}}_q(n_x) \right) - \widehat{\mathbf{r}}^\ell(n_r^\ell) \right\|^2 \leq D_{\max}$ ;
10    end
11    Evaluate  $n_r(n_x) = \min_\ell \underline{n}_r^\ell$  and  $\underline{\ell} = \arg \min_\ell \underline{n}_r^\ell$ ;
12    if  $n_x + n_r(n_x) < n_{\max}$  then
13       $n_{\max} = n_x + n_r(n_x)$ ;
14       $\mathcal{N}_x^m = [0, n_{\max} - n_{\min}^m]$ 
15       $\widehat{n}_x = n_x; \widehat{n}_r = n_r(n_x); \widehat{m} = m; \widehat{\ell} = \underline{\ell}$ ;           /* Update output */
16    end
17  end
18 end

```

---

If the compression approach  $\ell$  is scalable, then the minimum value  $n_r^\ell$  is easily obtained at line 8 of Algorithm 1 via a single encoding step. The value of  $n_{\max}$  may decrease from one model to another, leading to a decrease of the size of the interval  $\mathcal{N}_x^m$ , as models are tested.

Regarding the complexity, for each model  $m \in \mathcal{M}$ , the estimate  $\hat{\theta}$  of the vector of parameters has to be evaluated only once. When the model output  $\mathbf{x}^m(\theta)$  is linear in  $\theta$ , an explicit expression can be used to obtain  $\hat{\theta}$ . When it is non-linear in  $\theta$ , an iterative search has to be performed. Then for each model, in the worst case,  $|\mathcal{N}_x^m|$  values for  $n_x$  have to be considered, where  $|\mathcal{N}_x^m|$  represents the cardinal number of the set  $\mathcal{N}_x^m$ . For each of these values, Proposition 2 yields the optimal bit allocation for the quantization of  $\hat{\theta}$  and  $\mathbf{x}^m(\hat{\theta}_q(n_x))$  has to be evaluated as well as the residual  $\mathbf{r}^m(\hat{\theta}_q(n_x))$ . Then,  $L$  residual compression methods have to be compared. Consequently, in a worst-case scenario, Algorithm 1 involves performing  $\sum_{m=1}^M L |\mathcal{N}_x^m|$  residual compressions.

#### D. Golden Section Search

For each model  $m \in \mathcal{M}$  and each value of  $n_x \in \mathcal{N}_x^m$ , Algorithm 2 evaluates  $n_r(n_x)$ , the minimum rate required in the second stage to reach the distortion target  $D_{\max}$ . In this section, we assume for each model  $m \in \mathcal{M}$  that  $n_x + n_r(n_x)$  is convex in  $n_x$ . Then we solve the optimization problem in (7) using the GSS method [98], see Algorithm 2. The function `Eval_nr` (lines 1–8) evaluates  $n_r(n_x)$  and the associated method  $\underline{\ell}$  at the second stage for given  $m$ ,  $\hat{\theta}$ ,  $n_x$ , and  $D_{\max}$ . This function corresponds to lines 8–11 of Algorithm 1. In Algorithm 2, for each model  $m \in \mathcal{M}$  (line 10),  $\hat{\theta}$  is evaluated (line 11), and the interval  $\mathcal{N}_x^m$  is initialized (line 13). Then, the `GoldenSectionSearch` algorithm (line 14) is applied to find the minimum of  $n_x + n_r(n_x)$  under the distortion constraint  $D^{m,\ell}(n_x, n_r) \leq D_{\max}$ . This function takes as input  $m$ ,  $\hat{\theta}$ ,  $\mathcal{N}_x^m$ , and  $D_{\max}$  and returns  $n_x$ ,  $n_r$ , and  $\underline{\ell}$  with less function evaluations than the ES. At each iteration of the GSS, the function `Eval_nr` is called to get, for a given value of  $n_x$ , the minimum of  $n_x + n_r(n_x)$  under the distortion constraint  $D^{m,\ell}(n_x, n_r) \leq D_{\max}$ .

If that value is less than  $n_{\max}$  (line 15), then  $\hat{n}_x$ ,  $\hat{n}_r$ ,  $\hat{m}$ , and  $\hat{\ell}$  are updated (line 16). Finally,  $n_{\max}$  is updated (line 17).

Regarding the complexity, for each model  $m \in \mathcal{M}$ , the estimate  $\hat{\theta}$  of the vector of parameters has to be evaluated only once. Then for each model, the GSS considers only  $\log_{1/\alpha}(|\mathcal{N}_x^m| - 1)$  values for  $n_x$ , where  $\alpha$  is the golden ratio. For each of these values, the optimal bit allocation for the quantization of  $\hat{\theta}$  has to be evaluated as well as the residual  $\mathbf{r}^m(\hat{\theta}_q(n_x))$ . Then,  $L$  residual compression methods have to be compared. Consequently, in a worst-case scenario,  $\sum_{m=1}^M L \log_{1/\alpha}(|\mathcal{N}_x^m| - 1)$  residual compression have to be performed. This is computationally less complex than the ES. In practice, since  $n_{\max}$  is updated for each model, the size  $|\mathcal{N}_x^m|$  may decrease with each tested model, thereby further reducing the overall computational cost compared to the worst-case scenario.

---

**Algorithm 2:** Solution for (7) using GSS

---

```

1 Function Eval_nr( $m, \hat{\theta}, n_x, D_{\max}$ )
2   Quantize  $\hat{\theta}$  to obtain  $\hat{\theta}_q(n_x)$  with bit allocation determined by Proposition 2 ;
3   for each  $\ell \in \mathcal{L}$  do
4     Find  $\underline{n}_r^\ell$ , the smallest value of  $n_r^\ell$  such that  $\frac{1}{N} \left\| \mathbf{x} - \mathbf{x}^m \left( \hat{\theta}_q(n_x) \right) - \hat{\mathbf{r}}^\ell(n_r^\ell) \right\|^2 \leq D_{\max}$ ;
5   end
6   Evaluate  $n_r(n_x) = \min_\ell \underline{n}_r^\ell$  and  $\underline{\ell} = \arg \min_\ell \underline{n}_r^\ell$ ;
7   return  $n_r(n_x), \underline{\ell}$ ;
8 end
9 Determine  $n_{\max}$  using (16) and  $\underline{\ell}$  using (18);
10 for  $m \in \mathcal{M}$  do
11   Evaluate  $\hat{\theta}$  using (1);
12   Evaluate  $n_{\min}^m$  using (20) ;
13   Initialize  $\mathcal{N}_x^m = [0, n_{\max} - n_{\min}^m]$ ;
14    $(n_x, n_r, \underline{\ell}) = \text{GoldenSectionSearch} \left( m, \hat{\theta}, \mathcal{N}_x^m, D_{\max} \right)$ ; /* Using Eval_nr */
15   if  $n_x + n_r < n_{\max}$  then
16      $\hat{n}_x = n_x, \hat{n}_r = n_r, \hat{m} = m, \hat{\ell} = \underline{\ell}$ ; /* Update output */
17      $n_{\max} = n_x + n_r$ 
18   end
19 end

```

---

## V. USING RATE-DISTORTION MODELS

In this section, two models of the distortion  $D^{m,\ell}(n_x, n_r)$  introduced in (8) are proposed. They are then exploited to obtain an approximate, reduced-complexity, solution of (7).

Section V-A introduces a first rate-distortion model assuming that the residuals are uncorrelated and Gaussian. A second model is proposed in Section V-B where temporal correlation of the residuals is taken into account. Using these models, Section V-C introduces an algorithm to select a subset of promising candidate models for the first compression stage and to estimate optimal values for  $n_x$  and  $n_r$  for each candidate model.

### A. Rate-Distortion Model Assuming Uncorrelated Gaussian Residuals

Assume that the  $N$  components of the residual  $\mathbf{r}^m \left( \hat{\theta}_q(n_x) \right) = \mathbf{x} - \mathbf{x}^m \left( \hat{\theta}_q(n_x) \right)$  obtained at the output of the first stage are modeled as realizations of independent and identically distributed zero-mean Gaussian variables with variance  $\left\| \mathbf{r}^m \left( \hat{\theta}_q(n_x) \right) \right\|^2 / N$ . Moreover, assuming that the second stage achieves

the rate-distortion bound for Gaussian sources [99], the distortion of the output of the second stage when  $n_r$  bits have been allocated is

$$D^{m,\ell}(n_x, n_r) = \frac{1}{N} \left\| \mathbf{r}^m \left( \widehat{\boldsymbol{\theta}}_q(n_x) \right) \right\|^2 2^{-2n_r/N}. \quad (23)$$

The model (23) and the following expressions of the rate-distortion models do not account for the type of encoder  $\ell$  used at the second stage. Consequently, the superscript  $\ell$  is omitted in  $D^{m,\ell}(n_x, n_r)$  in what follows.

The norm of  $\mathbf{r}^m \left( \widehat{\boldsymbol{\theta}}_q(n_x) \right)$  has to be evaluated for each  $n_x$ , which is one of the sources of complexity of the algorithms presented in Section IV. To address this issue, we first rewrite the residual as

$$\mathbf{r}^m \left( \widehat{\boldsymbol{\theta}}_q(n_x) \right) = \mathbf{x} - \mathbf{x}^m \left( \widehat{\boldsymbol{\theta}} \right) + \mathbf{x}^m \left( \widehat{\boldsymbol{\theta}} \right) - \mathbf{x}^m \left( \widehat{\boldsymbol{\theta}}_q(n_x) \right) \quad (24)$$

$$= \mathbf{r}^m \left( \widehat{\boldsymbol{\theta}} \right) + \mathbf{e}_q^m(\widehat{\boldsymbol{\theta}}, n_x) \quad (25)$$

where  $\mathbf{r}^m \left( \widehat{\boldsymbol{\theta}} \right) = \mathbf{x} - \mathbf{x}^m \left( \widehat{\boldsymbol{\theta}} \right)$  represents the error due to the inaccuracy of the model (without parameter quantization) and  $\mathbf{e}_q^m(\widehat{\boldsymbol{\theta}}, n_x) = \mathbf{x}^m(\widehat{\boldsymbol{\theta}}) - \mathbf{x}^m \left( \widehat{\boldsymbol{\theta}}_q(n_x) \right)$  represents the contribution to the residual of the model parameter quantization error.

In general, one has

$$2 \left| \langle \mathbf{r}^m \left( \widehat{\boldsymbol{\theta}} \right), \mathbf{e}_q^m(\widehat{\boldsymbol{\theta}}, n_x) \rangle \right| \ll \left\| \mathbf{r}^m \left( \widehat{\boldsymbol{\theta}} \right) \right\|^2 + \left\| \mathbf{e}_q^m(\widehat{\boldsymbol{\theta}}, n_x) \right\|^2, \quad (26)$$

so that  $\mathbf{r}^m \left( \widehat{\boldsymbol{\theta}} \right)$  and  $\mathbf{e}_q^m(\widehat{\boldsymbol{\theta}}, n_x)$  can be assumed as uncorrelated. Consequently, (23) can be rewritten as

$$D^m(n_x, n_r) = \frac{1}{N} \left( \left\| \mathbf{r}^m \left( \widehat{\boldsymbol{\theta}} \right) \right\|^2 + \left\| \mathbf{e}_q^m(\widehat{\boldsymbol{\theta}}, n_x) \right\|^2 \right) 2^{-2n_r/N}. \quad (27)$$

### B. Rate-Distortion Model Assuming Correlated Gaussian Residuals

In practice, for a signal  $\mathbf{x}$  and a model  $m$ , the successive samples of  $\mathbf{r}^m(n_x)$  may exhibit some correlation. The aim of DCT, DWT, or VAE at the second compression stage is to efficiently decorrelate the residual prior to quantization and entropy coding. In this section, the temporal correlation between the samples of both  $\mathbf{r}^m(\widehat{\boldsymbol{\theta}})$  and  $\mathbf{e}_q^m(\widehat{\boldsymbol{\theta}}, n_x)$ , introduced in (25), is taken into account to get a more accurate rate-distortion model.

To account for the temporal correlation between samples, the components of the vector  $\mathbf{r}^m(\widehat{\boldsymbol{\theta}}) = (r_1^m(\widehat{\boldsymbol{\theta}}), \dots, r_N^m(\widehat{\boldsymbol{\theta}}))$  are modeled as realizations of an Autoregressive (AR) process

$$r_n^m(\widehat{\boldsymbol{\theta}}) = \sum_{p=1}^{P_m} \alpha_{m,p}^m r_{n-p}^m(\widehat{\boldsymbol{\theta}}) + \varepsilon_{m,n}^m, \quad (28)$$

where  $P_m$  and  $\alpha_{m,p}^m$  represent the order and coefficients of the AR process and  $\varepsilon_{m,n}^m$  represents realizations of zero-mean uncorrelated Gaussian variables with variance  $(\sigma_m^m)^2$ . Similarly, for the components of  $\mathbf{e}_q^m(\widehat{\boldsymbol{\theta}}, n_x) = (e_{q,1}^m(\widehat{\boldsymbol{\theta}}, n_x), \dots, e_{q,N}^m(\widehat{\boldsymbol{\theta}}, n_x))^T$ , the following model is considered

$$e_{q,n}^m(\widehat{\boldsymbol{\theta}}, n_x) = \sum_{p=1}^{P_q} \alpha_{q,p}^m e_{q,n-p}^m(\widehat{\boldsymbol{\theta}}, n_x) + \varepsilon_{q,n}^m(n_x), \quad (29)$$

where  $P_q$  and  $\alpha_{q,p}^m$  represent the order and coefficients of the AR process, and the  $\varepsilon_{q,n}^m(\hat{\boldsymbol{\theta}}, n_x)$  are realizations of zero-mean uncorrelated Gaussian noise with variance  $(\sigma_q^m)^2(n_x)$ . The variances  $(\sigma_m^m)^2$  and  $(\sigma_q^m)^2(n_x)$  are determined using estimates of the autocorrelation functions  $\gamma_m^m(p)$  and  $\gamma_q^m(p, n_x)$  of  $r_n^m(\hat{\boldsymbol{\theta}})$  and  $e_{q,n}^m(\hat{\boldsymbol{\theta}}, n_x)$  via Yule-Walker equations [100] to obtain

$$\begin{pmatrix} \alpha_{m,1}^m \\ \vdots \\ \alpha_{m,P_m}^m \\ (\sigma_m^m)^2 \end{pmatrix} = \begin{pmatrix} \gamma_m^m(1) & \dots & \gamma_m^m(P_m) & 1 \\ \gamma_m^m(0) & \dots & \gamma_m^m(P_m-1) & 0 \\ \vdots & \ddots & \vdots & \vdots \\ \gamma_m^m(P_m-1) & \dots & \gamma_m^m(0) & 0 \end{pmatrix}^{-1} \begin{pmatrix} \gamma_m^m(0) \\ \vdots \\ \gamma_m^m(P_m) \end{pmatrix}, \quad (30)$$

and

$$\begin{pmatrix} \alpha_{q,1}^m \\ \vdots \\ \alpha_{q,P_q}^m \\ (\sigma_q^m)^2(n_x) \end{pmatrix} = \begin{pmatrix} \gamma_q^m(1, \hat{\boldsymbol{\theta}}, n_x) & \dots & \gamma_q^m(P_q, \hat{\boldsymbol{\theta}}, n_x) & 1 \\ \gamma_q^m(0, \hat{\boldsymbol{\theta}}, n_x) & \dots & \gamma_q^m(P_q-1, \hat{\boldsymbol{\theta}}, n_x) & 0 \\ \vdots & \ddots & \vdots & \vdots \\ \gamma_q^m(P_q-1, \hat{\boldsymbol{\theta}}, n_x) & \dots & \gamma_q^m(0, \hat{\boldsymbol{\theta}}, n_x) & 0 \end{pmatrix}^{-1} \begin{pmatrix} \gamma_q^m(0, n_x) \\ \vdots \\ \gamma_q^m(P_q, n_x) \end{pmatrix}. \quad (31)$$

Then, assuming that the second compression stage is able to perfectly decorrelate the components of  $r_n^m(\hat{\boldsymbol{\theta}})$  and  $e_{q,n}^m(\hat{\boldsymbol{\theta}}, n_x)$  so that only  $\varepsilon_{m,n}$  and  $\varepsilon_{q,n}(n_x)$  have to be compressed, and that the second stage achieves the rate-distortion bound for uncorrelated Gaussian sources, the distortion can be modeled as

$$D^m(n_x, n_r) = \left( (\sigma_m^m)^2 + (\sigma_q^m)^2(n_x) \right) 2^{-2n_r/N}. \quad (32)$$

For example, if  $r^m(\hat{\boldsymbol{\theta}})$  and  $e_q^m(\hat{\boldsymbol{\theta}}, n_x)$  are represented by first-order AR models, (32) boils down to

$$D^m(n_x, n_r) \simeq \left( \frac{\hat{\gamma}_m^m(0)^2 - \hat{\gamma}_m^m(1)^2}{\hat{\gamma}_m^m(0)} + \frac{\hat{\gamma}_q^m(0, \hat{\boldsymbol{\theta}}, n_x)^2 - \hat{\gamma}_q^m(1, \hat{\boldsymbol{\theta}}, n_x)^2}{\hat{\gamma}_q^m(0, \hat{\boldsymbol{\theta}}, n_x)} \right) 2^{-2n_r/N}. \quad (33)$$

For a given vector  $\mathbf{x}$  and model  $m$ ,  $\hat{\boldsymbol{\theta}}$  has to be evaluated once. This is also the case for the biased estimate

$$\hat{\gamma}_m^m(p) = \frac{1}{N} \sum_{n=p+1}^N r_n^m(\hat{\boldsymbol{\theta}}) r_{n-p}^m(\hat{\boldsymbol{\theta}}) \quad (34)$$

of the autocorrelation function  $\gamma_m^m(p)$  of  $r_n^m(\hat{\boldsymbol{\theta}})$ , from which  $(\sigma_m^m)^2$  is deduced using (30). Nevertheless,  $e_q^m(\hat{\boldsymbol{\theta}}, n_x)$  and the estimate of its autocorrelation function  $\hat{\gamma}_q^m(p, \hat{\boldsymbol{\theta}}, n_x)$  have still to be evaluated for each  $n_x$ . Proposition 3 simplifies the evaluation of  $\hat{\gamma}_q^m(p, \hat{\boldsymbol{\theta}}, n_x)$ .

**Proposition 3.** Consider a model with output  $\mathbf{x}^m(\boldsymbol{\theta})$  and assume that the components of the quantization error  $\varepsilon(\hat{\boldsymbol{\theta}}, n_x) = \hat{\boldsymbol{\theta}} - \hat{\boldsymbol{\theta}}_q(n_x)$  of the estimated parameter vector  $\hat{\boldsymbol{\theta}}$  are zero-mean and uncorrelated then

$$\hat{\gamma}_q^m(p, \hat{\boldsymbol{\theta}}, n_x) = \sum_{k=1}^K h_k^m(p, \hat{\boldsymbol{\theta}}) \sigma_k^2(\hat{\boldsymbol{\theta}}, n_x), \quad (35)$$

where

$$h_k^m(p, \hat{\boldsymbol{\theta}}) = \frac{1}{N} \sum_{n=p+1}^N \frac{\partial x_n^m(\hat{\boldsymbol{\theta}})}{\partial \hat{\theta}_k} \frac{\partial x_{n-p}^m(\hat{\boldsymbol{\theta}})}{\partial \hat{\theta}_k} \quad (36)$$

and

$$\sigma_k^2(\hat{\boldsymbol{\theta}}, n_x) = \mathbb{E}(\varepsilon_k^2(\hat{\boldsymbol{\theta}}, n_x)) \quad (37)$$

is the variance of the  $k$ -th component of  $\varepsilon(\hat{\boldsymbol{\theta}}, n_x)$ .

*Proof.* See Appendix A.  $\square$

The term  $h_k(p, \hat{\boldsymbol{\theta}})$  in (36) is the expected value of the autocorrelation function of the sensitivity of the model output with respect to the  $k$ -th component of  $\hat{\boldsymbol{\theta}}$ . The estimate  $\hat{\gamma}_q^m(p, \hat{\boldsymbol{\theta}}, n_x)$  is then obtained as a weighted average of  $h_k^m(p, \hat{\boldsymbol{\theta}})$ , where the weights are given by the variances of the quantization error of each component of the estimated parameter vector.

The following corollaries provide expressions of  $h_k(p, \hat{\boldsymbol{\theta}})$  for different models.

**Corollary 4.** For a sinusoidal model with parameter vector  $\hat{\boldsymbol{\theta}} = (\hat{a}, \hat{f}, \hat{\phi})^T$ ,

$$\begin{aligned} h_1(p, \hat{\boldsymbol{\theta}}) &= \frac{1}{N} \sum_{n=p+1}^N \cos(2\pi\hat{f}nT_s + \hat{\phi}) \cos(2\pi\hat{f}(n-p)T_s + \hat{\phi}) \\ &= \frac{1}{2N} \left( \cos(2\pi\hat{f}(N+1)T_s + 2\hat{\phi}) \frac{\sin(2\pi\hat{f}(N-p)T_s)}{\sin(2\pi\hat{f}T_s)} + (N-p) \cos(2\pi\hat{f}pT_s) \right), \end{aligned} \quad (38)$$

$$h_2(p, \hat{\boldsymbol{\theta}}) = \frac{4\pi^2 T_s^2 \hat{a}^2}{N} \sum_{n=p+1}^N n(n-p) \sin(2\pi\hat{f}nT_s + \hat{\phi}) \sin(2\pi\hat{f}(n-p)T_s + \hat{\phi}), \quad (39)$$

$$\begin{aligned} h_3(p, \hat{\boldsymbol{\theta}}) &= \frac{\hat{a}^2}{N} \sum_{n=p+1}^N \sin(2\pi\hat{f}nT_s + \hat{\phi}) \sin(2\pi\hat{f}(n-p)T_s + \hat{\phi}) \\ &= \frac{\hat{a}^2}{2N} \left( -\cos(2\pi\hat{f}(N+1)T_s + 2\hat{\phi}) \frac{\sin(2\pi\hat{f}(N-p)T_s)}{\sin(2\pi\hat{f}T_s)} + (N-p) \cos(2\pi\hat{f}pT_s) \right). \end{aligned} \quad (40)$$

*Proof.* See Appendix B.  $\square$

**Corollary 5.** For a Tchebychev polynomial model of degree  $K-1$  and parameter vector  $\hat{\boldsymbol{\theta}}$ ,

$$h_k(p, \hat{\boldsymbol{\theta}}) = \frac{1}{N} \sum_{n=p+1}^N \mathcal{T}_k\left(2\frac{n}{N}-1\right) \mathcal{T}_k\left(2\frac{n-p}{N}-1\right), \quad (41)$$

for  $k = 0, \dots, K-1$ .

*Proof.* See Appendix C.  $\square$

**Corollary 6.** For a sample predictive model of order  $K$  and offset  $\eta$ ,

$$h_k(p) = \frac{1}{N} \sum_{n=p+1}^N \hat{x}_{(i-1)N+n-\eta-k+1} \hat{x}_{(i-1)N+n-p-\eta-k+1}, \quad (42)$$

for  $k = 1, \dots, K$ .

*Proof.* See Appendix D.

For parameter predictive model described in Section IV-A, the entries of  $\widehat{\boldsymbol{\delta}}$  are scalar quantized to get  $\widehat{\boldsymbol{\delta}}_q = \widehat{\boldsymbol{\delta}} + \boldsymbol{\varepsilon}$ , where  $\boldsymbol{\varepsilon}$  is the quantization error vector. Consequently,  $h_k(p)$ ,  $k = 1, \dots, K$  can be evaluated considering  $\widehat{\boldsymbol{\delta}}$  instead of  $\widehat{\boldsymbol{\theta}}$ , whatever the model.  $\square$

### C. Reduced-Complexity Search

The following reduced-complexity search algorithm exploits, for each model  $m \in \mathcal{M}$ , the analytical model  $D^m(n_x, n_r)$ , either given by (27) or by (32) to get an approximate solution of (7) by solving

$$\begin{aligned} \underline{n}_x^m, \underline{n}_r^m &= \arg \min_{n_x, n_r} n_h + n_x + n_r \\ \text{s.t. } D^m(n_x, n_r) &\leq D_{\max}. \end{aligned} \quad (43)$$

Since  $D^m(n_x, n_r)$  is only an approximation of  $D^{m,\ell}(n_x, n_r)$ , an exhaustive or a GSS is then performed considering a subset  $\mathcal{M}' \subset \mathcal{M}$  of most promising models, *i.e.*, of models with the smallest  $\underline{n}_x^m + \underline{n}_r^m$ . For each of these models, a subset  $\mathcal{N}'^m$  of values around  $\underline{n}_x^m$  is also considered to account for the model inaccuracy.

Algorithm 3 takes  $\boldsymbol{x}$  as input and outputs the subset  $\mathcal{M}'$  and the set  $\mathcal{N}'^m$  for each  $m \in \mathcal{M}'$ . For each model  $m$  (line 1),  $\widehat{\boldsymbol{\theta}}$  and  $\mathbf{r}^m(\widehat{\boldsymbol{\theta}})$  are evaluated at line 2 and the variance  $(\sigma_m^m)^2$  using (30) (line 3 and 4). The variable  $n_{\max}$ , which stores the minimum number of bits required for compression, is initialized to infinity (line 5). For each value of  $n_x$ , starting from zero (lines 6 and 7), then  $(\sigma_q^m)^2(n_x)$  is determined using (31) at line 8, as detailed in Section V. Based on this value, the corresponding  $n_r$  is obtained by solving 43 and imposing  $D^m(n_x, n_r) \leq D_{\max}$  in (32), to get

$$n_r(n_x) = \left\lceil \frac{N}{2} \log_2 \left( \frac{(\sigma_m^m)^2 + (\sigma_q^m)^2(n_x)}{D_{\max}} \right) \right\rceil, \quad (44)$$

see line 8. Assuming that  $n_x + n_r(n_x)$  is convex, if  $n_x + n_r(n_x) < n_{\max}$ ,  $n_{\max}$  is updated (line 10). The process then increments  $n_x$  (line 12), and the candidate output values  $\underline{n}_x^m$  and  $\underline{n}_r^m$  are updated with the values  $n_x$  and  $n_r$  (line 11). The process stops when  $n_x + n_r(n_x) \geq n_{\max}$  (line 13), and the set

$$\mathcal{N}'^m = [\underline{n}_x^m - \lfloor \Delta_{nx}/2 \rfloor, \underline{n}_x^m + \lfloor \Delta_{nx}/2 \rfloor], \quad (45)$$

of candidates for  $\widehat{n}_x$  is formed (line 14) to perform some refined search around  $\underline{n}_x^m$ .

Once all models have been processed, a subset  $\mathcal{M}' \subset \mathcal{M}$  containing the  $\Delta_{\mathcal{M}} \leq M$  most promising models indexes is formed (line 18). A reduced complexity ES or GSS may then be performed considering all  $m \in \mathcal{M}'$  and all  $n_x \in \mathcal{N}'^m$ .

---

**Algorithm 3:** Preselection of candidate models and  $n_x$  values

---

```

1 for each  $m \in \mathcal{M}$  do
2   Evaluate  $\hat{\theta}$  and  $\mathbf{r}^m(\hat{\theta}) = \mathbf{x} - \mathbf{x}^m(\hat{\theta})$  using (1)\;
3   Evaluate an estimate  $\hat{\gamma}_m^m(p)$  of  $\gamma_m^m(p)$  from  $\mathbf{r}^m(\hat{\theta})\backslash$ ;
4   Evaluate  $(\sigma_m^m)^2$  from  $\hat{\gamma}_m^m(p)$  using (30)\;
5    $n_{\max} = \infty$ ;
6    $n_x = 0$ ;
7   while true do
8     Use offline estimate of  $(\sigma_q^m)^2(n_x)$  using (31) to get
9       
$$n_r(n_x) = \left\lceil \frac{N}{2} \log_2 \left( \frac{(\sigma_m^m)^2 + (\sigma_q^m)^2(n_x)}{D_{\max}} \right) \right\rceil$$

10    tcc* Solve (43) using (32)
11    if  $n_x + n_r(n_x) < n_{\max}$  then
12       $n_{\max} = n_x + n_r(n_x)$ ;
13       $\underline{n}_x^m = n_x$  ;  $\underline{n}_r^m = n_r(n_x)$  ;
14       $n_x = n_x + 1$  ;
15    else
16       $\mathcal{N}_x'^m = [\underline{n}_x^m - \lfloor \frac{\Delta_{nx}}{2} \rfloor, \underline{n}_x^m + \lfloor \frac{\Delta_{nx}}{2} \rfloor]$  Break;
17    end
18  end
19 end
20 Build  $\mathcal{M}' \subset \mathcal{M}$  of the  $\Delta_M$  model indexes with smallest  $\underline{n}_x^m + \underline{n}_r^m$ .

```

---

This approach reduces the computational cost by limiting the search space for  $n_x$ . In a worst-case scenario, the number of residual compression methods to evaluate is

$$\sum_{m=1}^{M'} L |\mathcal{N}_x'^m| = \Delta_M L \Delta_{nx} \quad (46)$$

when using ES (see Section IV-C), and  $\Delta_M L \log_{1/\alpha}(\Delta_{nx})$  with the GSS (see Section IV-D). The computational cost is controlled via the choice of  $\Delta_M$  and  $\Delta_{nx}$ .

## VI. EXPERIMENTS

Section VI-A introduces the simulation setup. In Section VI-B, the validity of several hypotheses considered in Sections IV-D, and V are evaluated. Then, Section VI-C shows the performance of the proposed Distortion Model (DM) in estimating  $\hat{n}_x$  and  $\hat{n}_r$  for a target distortion  $D_{\max}$  for different values

of  $\Delta_{nx}$  and  $\Delta_M$ . In Section VI-D, the compression performance for different values of  $D_{max}$  and window sizes is compared with three reference methods considering a large database of signal samples. Specifically, we analyze the ES approach in Section IV-C, the GSS approach in Section IV-D, and the ES approach with DM as well as the ES approach with GSS in Section V-C <sup>1</sup>.

### A. Simulation set-up

Twelve three-phase voltage signals from the digital-fault-recording-database [84] acquired on the French electrical grid are first considered. The selected signals correspond to indices 85, 91, 98, 176, 189, 195, 282, 287, 316, 337, 371, and 380, as they represent typical faults. All signals last one second and are sampled at 6400 Hz (128 samples per nominal period  $f_n = 50$  Hz). The length of the window is set to  $N = 128$  samples. Consequently, each signal is partitioned into 50 non-overlapping windows of 20 ms duration, leading to a total of 1800 vectors to compress. More extensive analyses have been performed on the signals with index 91 and 337 from [84].

Table I summarizes the different models used in the first and second stages of the considered MMC approach. For the polynomial model, we choose uniform prior distributions  $p_\theta$  over intervals with widths  $w_{K^m}$  for the  $k$ -th coefficient of the polynomial model  $m$ . The values of  $w_{K^m}$  were determined to gather 90 % of the distribution of  $\theta_{K^m}$ , based on an analysis of 20,000 signals of 128 samples from [84].

Model	Definitions	$p_\theta$
Bypass		
Sinusoidal	2	$\mathcal{U} \left( \boldsymbol{\theta}; \begin{pmatrix} 0.5 \\ 40.9 \\ -\pi \end{pmatrix}, \begin{pmatrix} 1 \\ 50.1 \\ \pi \end{pmatrix} \right)$
Poly. of order $K \in [0, \dots, 9]$	3	$\mathcal{U} \left( \boldsymbol{\theta}; -\begin{pmatrix} \frac{w_1^m}{2} \\ \dots \\ \frac{w_{K+1}^m}{2} \end{pmatrix}, \begin{pmatrix} \frac{w_1^m}{2} \\ \dots \\ \frac{w_{K+1}^m}{2} \end{pmatrix} \right)$
Sample pred., order $K \in [1, 2]$ , $\eta = 0$	4	$\mathcal{U} \left( \boldsymbol{\theta}; -\frac{1}{2} \mathbf{1}, \frac{1}{2} \mathbf{1} \right)$
Parameter pred.	5	$\mathcal{U} \left( \boldsymbol{\delta}; -0.1 \cdot \mathbf{1}, 0.1 \cdot \mathbf{1} \right)$

TABLE I

MMC APPROACH: MODEL TYPES AND *a priori* DISTRIBUTIONS FOR THE MODEL PARAMETERS CONSIDERED IN THE FIRST STAGE;  $\mathcal{U}(\boldsymbol{\theta}; \mathbf{a}, \mathbf{b})$  REPRESENTS A UNIFORM DISTRIBUTION OVER THE BOX WITH CENTER  $0.5(\mathbf{a} + \mathbf{b})$  WITH WIDTHS  $\mathbf{b} - \mathbf{a}$ ; THE VECTOR  $\mathbf{1}$  IS A VECTOR OF ONES OF THE SAME DIMENSION AS  $\boldsymbol{\theta}$ .

In the second compression stage, two scalable methods for residual compression are considered, namely DCT followed by the Bit-Plane Coding (BPC) described in [83] and DWT followed by the EZW approach of [82].

The preamble of each compressed data packet is organized as follows. To represent one of the 15 model indexes,  $n_m = 4$  bits are required, and  $n_\ell = 1$  bit is used to indicate the residual compression method.

<sup>1</sup>Codes are available at: <https://github.com/CorentinPresvots/MMC-with-Quality-Constraint>

The number of bits  $n_{nx}$  indicating the length of the model parameter field depends on the chosen model  $m$  and its number of parameters  $K^m$ . We limit the number of bits per parameter to 12; consequently,  $n_{nx} = \lceil \log_2 (12K^m) \rceil$ , where  $\lceil \cdot \rceil$  represents rounding upwards. If the first compression stage is bypassed, no bits are required to represent  $n_x$ .

The number of bits  $n_{nr}$  indicating the length of the residual field depends on the chosen model  $\ell$ . If the second stage is bypassed, no bits are required to represent  $n_r$  and  $n_{kr}$ . The number of bits for each parameter is determined from the model index  $m$  and  $n_x$ , as detailed in Section IV-A.

For the number of bits  $n_{kx}$  required to represent the first scaling factor  $k_x$ , we assume that the absolute value of the phase-to-ground voltage is between 0.5 V and 500 kV. Since  $2^{-k_x}x \in [0.5, 1[$  for all  $x \in [0.5, 5 \cdot 10^5]$ , it follows that  $k_x \in \mathbb{K}_x = [0, \dots, 19]$ , leading to  $n_{kx} = 5$  bits.

If the maximum absolute value of the residual is less than  $10^{-3}$ , the residual is not encoded. Since the maximum amplitude of the scaled signal is in  $[0.5, 1[$ , a relative error of less than 0.1% of nominal voltage is obtained, which corresponds to the usual precision class of transformer instruments described in the International Electrotechnical Commission (IEC) 60044-1 standard [101], *i.e.*, less than  $\pm 90$  V.

For the number of bits  $n_{kr}$  required to represent the second scaling factor  $k_r$ , we require that  $2^{-k_r}r \in [0.5, 1[$  for all  $r \in [10^{-3}, 1]$ . This leads to  $k_r \in \mathbb{K}_r = [-9, \dots, 0]$  and  $n_{kr} = 4$  bits.

### B. Analysis of the considered hypotheses

Figure 3 illustrates three test signals in blue, each containing 128 samples corresponding to 20 ms of data extracted from the signals with index 91 and 337 in [84]. These signals are representative of transient behaviors. They are considered to evaluate the validity of various hypotheses considered in Sections V, IV-D, and V.

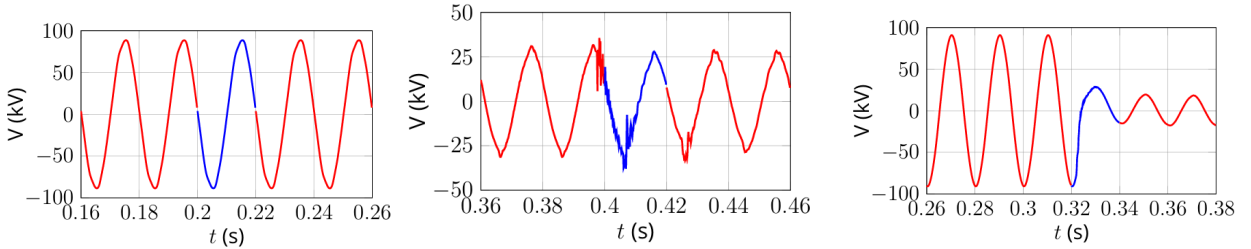


Fig. 3. Three test signals of 128 samples (blue curves, sampling rate  $f_s = 6400$  Hz) extracted from the database [84]; The first two signals are from the first phase of the signal with index 91, and the third from the second phase of the signal with index 337.

In the following section, we consider  $D_{\max} = 200^2 \text{ V}^2$ .

1) *Convexity of  $n_x + n_r(n_x)$  as a function of  $n_x$  under a constraint  $D_{\max}$* : In Section IV-D, we assume that  $n_x + n_r(n_x)$  is convex with respect to  $n_x$  to apply the GSS and find  $\hat{n}_x$ . Figure 4 represents  $n_x + n_r(n_x)$  as a function of  $n_x$  obtained by an ES (plain) and by the models (27) (dashed) and (33) (dotted) of  $n_x + n_r(n_x)$ , considering the three test signals and different signal models. Only the global shape is convex, but there

are irregularities, especially at low bit rates. This is mainly due to the fact that adding one extra bit to represent the model parameters does not always yield a residual easier to encode at the second stage. These irregularities lead to degraded performance of the GSS compared to the ES, as will be seen in Section VI-D.

The model (33) provides usually better results than (27). Even if there is some bias in the value of  $n_x + n_r(n_x)$ , the minimum obtained considering (33) is closer to the minimum obtained by ES than that obtained using (27).

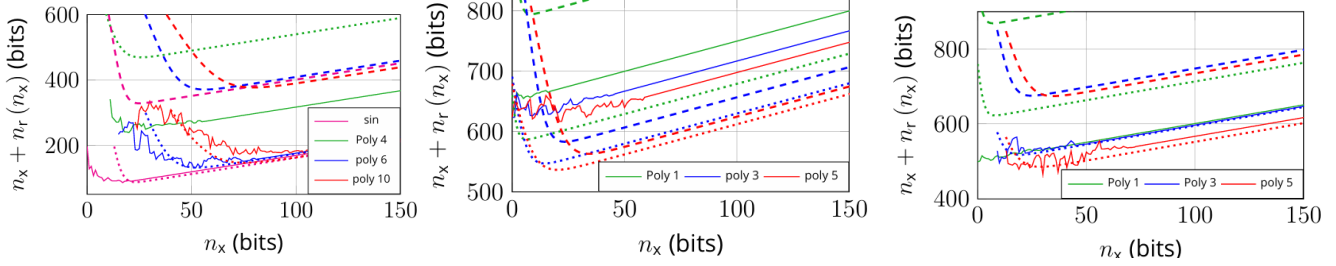


Fig. 4. Evolution of  $n_x + n_r(n_x)$  obtained by ES (plain), the model (27) (dashed), and (33) (dotted), as a function of  $n_x$  using sinusoidal (pink), polynomial models of degree 4 (green), 6 (blue), and 10 (red) with test signal 1 (left), and polynomial models of degree 1 (green), 3 (blue), and 5 (red) with test signals 2 (middle) and 3 (right) under a distortion constraint of  $D_{\max} = 200^2 \text{ V}^2$ .

2) *Evaluation of (27):* In Section V-A, we assume that

$$2 \left| \langle \mathbf{r}^m(\hat{\theta}), \mathbf{e}_q^m(\hat{\theta}, n_x) \rangle \right| \ll \left\| \mathbf{r}^m(\hat{\theta}) \right\|^2 + \left\| \mathbf{e}_q^m(\hat{\theta}, n_x) \right\|^2, \quad (47)$$

which underlies (27). For the two considered test signals, Figure 5 shows that this condition holds for all values of  $n_x$ .

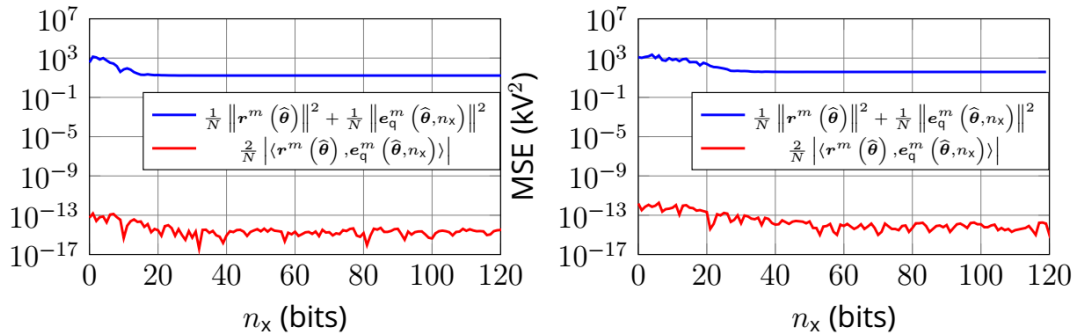


Fig. 5. Evolution of  $\frac{1}{N} \left\| \mathbf{r}^m(\hat{\theta}) \right\|^2 + \frac{1}{N} \left\| \mathbf{e}_q^m(\hat{\theta}, n_x) \right\|^2$  (blue) and  $\frac{2}{N} \left| \langle \mathbf{r}^m(\hat{\theta}), \mathbf{e}_q^m(\hat{\theta}, n_x) \rangle \right|$  (red), both as a function of  $n_x$ , using a 3th-degree polynomial model for the second test signal (middle) and a 5rd-degree polynomial for the third test signal (right) shown in Figure 3.

3) *Evaluation of (32):* In Section V-B, we assume that the components of the estimation residual  $\mathbf{r}^m(\hat{\theta})$  may exhibit temporal correlation. Figure 6 shows  $\mathbf{r}^m(\hat{\theta})$  and its Partial Autocorrelation Function (PACF) for the first test signal and a sinusoidal model, indicating a significant correlation. Figure 8 and 8

present the corresponding results for the second and third test signals, using polynomial models of degree 5 and 3, respectively.

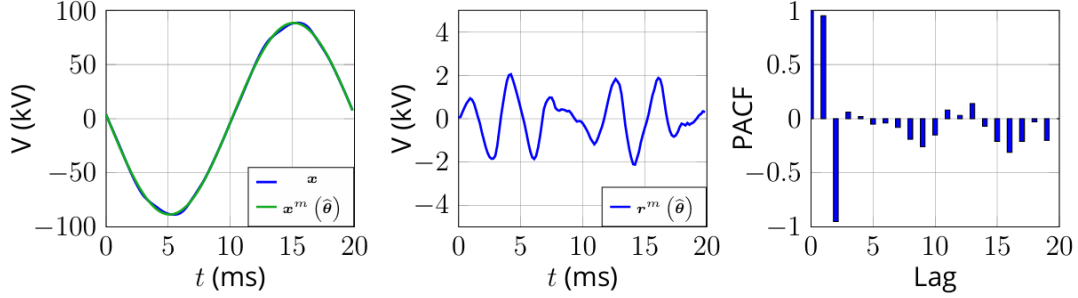


Fig. 6. For test signal 1 shown in Figure 3. Left: The test signal (blue) and its reconstruction using a sinusoidal model with unquantized parameters (green). Middle:  $r^m(\hat{\theta})$ . Right: PACF of  $r^m(\hat{\theta})$ .

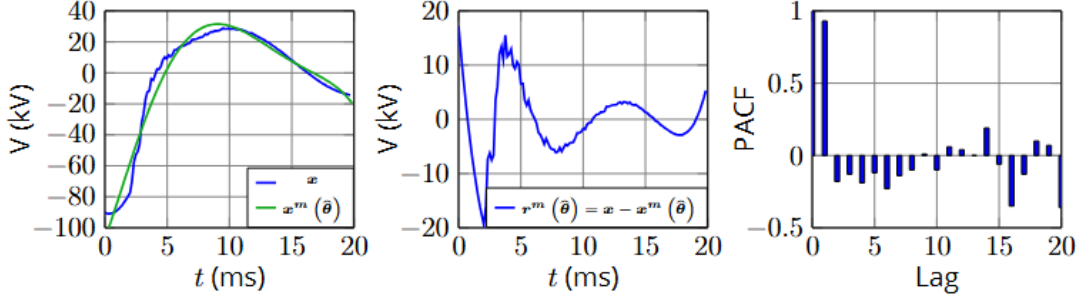


Fig. 7. For test signal 3 shown in Figure 3: test signal in blue and its reconstruction using a 5th-degree polynomial model with unquantized parameters in green (left),  $r^m(\hat{\theta})$  (middle), and PACF of  $r^m(\hat{\theta})$  (right).

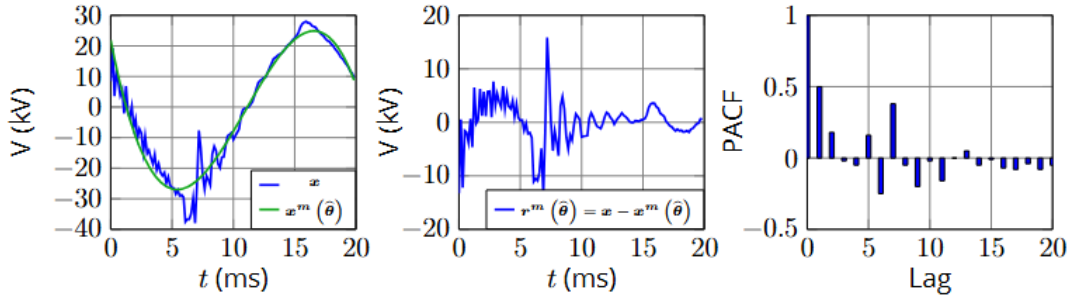


Fig. 8. For test signal 3 shown in Figure 3: test signal in blue and its reconstruction using a 3rd-degree polynomial model with unquantized parameters in green (left),  $r^m(\hat{\theta})$  (middle), and PACF of  $r^m(\hat{\theta})$  (right).

Similarly, the components of the quantization error  $e_q^m(\hat{\theta}, n_x)$  are correlated, as seen in Figures 9 and 10. This is confirmed by the PACF for different values of  $n_x$  which is significant at lag 1.

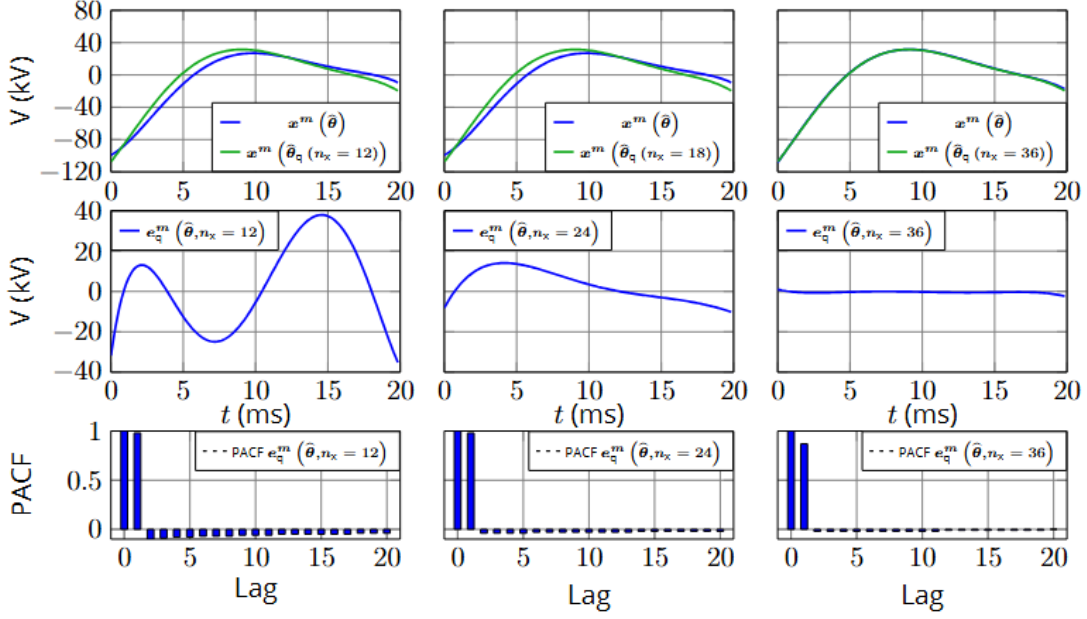


Fig. 9. First row: Reconstructed signal 1 (see Figure 3) using a polynomial model of degree 5 without parameter quantization (green), and with parameters quantized with  $n_x = 12$  bits (left), 24 bits (middle), and 36 bits (right) (blue). Second row: Quantization error  $e_q^m(\hat{\theta}, n_x)$  for parameter quantization with  $n_x = 12$  bits (left), 24 bits (middle), and 36 bits (right). Third row: PACF of  $e_q^m(\hat{\theta}, n_x)$  with parameters quantized with  $n_x = 12$  bits (left), 24 bits (middle), and 36 bits (right).

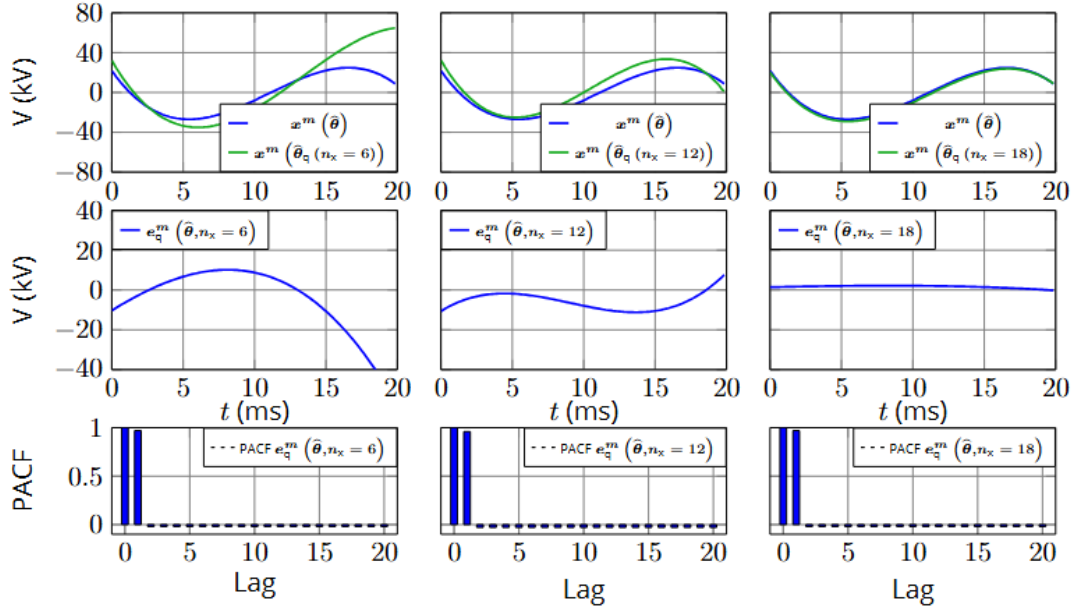


Fig. 10. First row: Reconstructed signal 2 (see Figure 3) using a polynomial of degree 3 without parameter quantization (green), and with parameters quantized to 6 bits (left), 12 bits (middle), and 18 bits (right) (blue). Second row: Quantization error  $e_q^m(\hat{\theta}, n_x)$  with parameter quantization at 6 bits (left), 12 bits (middle), and 18 bits (right). Third row: PACF of  $e_q^m(\hat{\theta}, n_x)$  with parameters quantization at 6 bits (left), 12 bits (middle), and 18 bits (right).

### C. Efficiency of the bit allocation and model selection

Figure 11 (left) shows the error between  $\hat{n}_x$  obtained using ES with Algorithm 1 and  $\underline{n}_x$  predicted by DM using Algorithm 3 when  $D_{\max} = 200^2 V^2$ . Figure 11 (right) shows the error between  $\hat{n}_{\text{tot}} = \hat{n}_x + \hat{n}_r$  obtained using ES and  $\underline{n}_{\text{tot}} = \underline{n}_x + \underline{n}_r$  predicted by DM. Different orders  $P_m$  and  $P_q$  of the AR model for the model error and quantization error are considered.

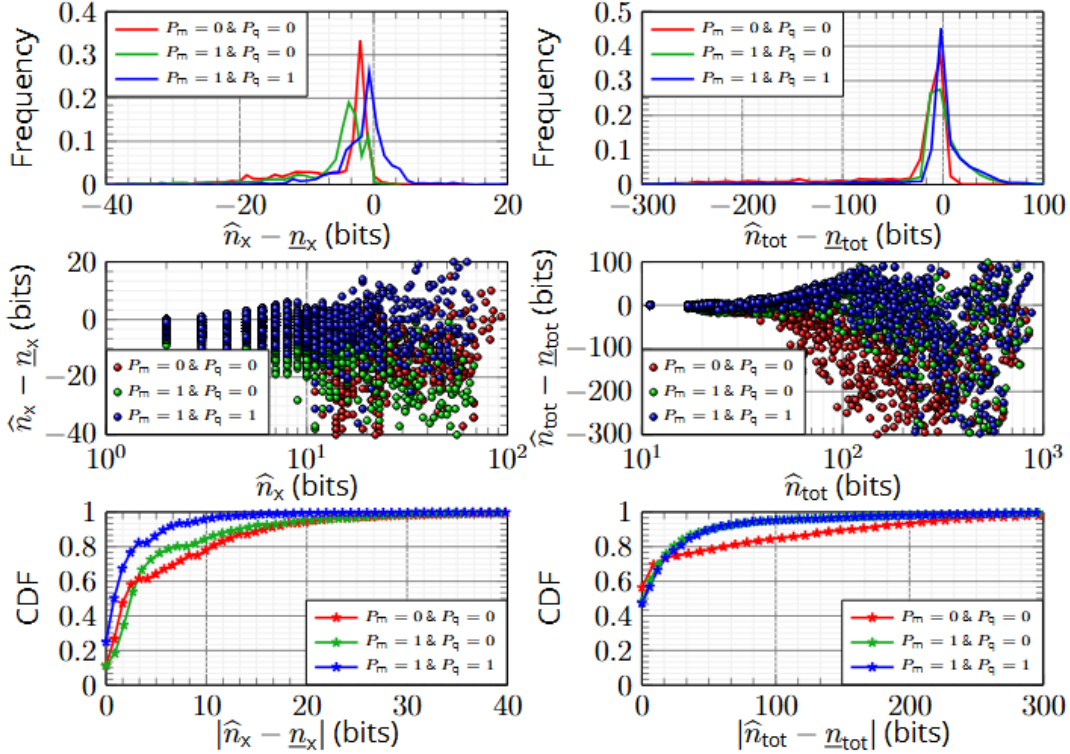


Fig. 11. First row: Histograms of the  $\hat{n}_x - \underline{n}_x$  (left) and  $\hat{n}_{\text{tot}} - \underline{n}_{\text{tot}}$  (right), where  $\hat{n}_x$  and  $\hat{n}_{\text{tot}}$  are obtained with using ES with Algorithm 1, and  $\underline{n}_x$  and  $\underline{n}_{\text{tot}} = \underline{n}_x + \underline{n}_r$  are obtained with DM with Algorithm 3, for different values of  $P_m$  and  $P_q$  based on the distortion model (32). Second row: Scatter plot showing the distribution of  $\hat{n}_x - \underline{n}_x$  (left) and  $\hat{n}_{\text{tot}} - \underline{n}_{\text{tot}}$  (right). Third row: CDF of the distribution of  $|\hat{n}_x - \underline{n}_x|$  (left) and  $|\hat{n}_{\text{tot}} - \underline{n}_{\text{tot}}|$  (right). Results are for  $D_{\max} = 200^2 V^2$ .

In Figure 11, the histograms (top row) and the CDFs (bottom row) alongside show that a first-order AR model of the residuals of the first stage enhance the prediction accuracy of  $\hat{n}_x$  using  $\underline{n}_x$  (left). For the prediction of  $\hat{n}_{\text{tot}}$  using  $\underline{n}_{\text{tot}}$  (right), we observe that considering  $P_m = 1$  significantly reduces the number of cases  $\underline{n}_{\text{tot}}$  overestimates  $\hat{n}_{\text{tot}}$ . Using  $P_q = 1$  instead of  $P_q = 0$ , does not provide significant improvement.

The scatter plots of Figure 11 (middle row) show that larger prediction errors are generally associated with signals requiring a high bit-rate to reach the target distortion. For the right scatter plot, we observe that the models with  $P_m = 1$ ,  $P_q = 1$  yields a less biased estimate of  $\hat{n}_x$ .

Initially, the set  $\mathcal{M}$  of 14 candidate models, see Table I. We compare the accuracy of model selection between the ES approach (Section IV-C) and the ES with DM (Section V-C). The impact of the number  $\Delta_M$  of models considered in the subset  $\mathcal{M}'$  of promising models evaluated by Algorithm 3, used to

initialize the set of models used by Algorithm 1. For the ES approach, Fig. 12 presents three confusion matrices for different values of  $\Delta_M$ . We can observe that increasing the number of retained models  $\Delta_M$  increases the percentage of model selections by the ES with DM approach which are similar to that of the ES approach. The ES approach achieves 87.6 bits per signal vector in average for a distortion constraint of  $D_{\max} = 200^2 V^2$ . The model prediction performance improves when  $\Delta_M$  increases. The average total bit rate also decreases from 92.6 bits per signal for  $\Delta_M = 1$  to 90.4 bits for  $\Delta_M = 2$ , and to 89.5 bits for  $\Delta_M = 3$ . By considering only 3 models out of the initial 14 for each signal, the reduced-complexity DM approach yields a computational cost reduction by a factor of at least 4 with an increase of the required rate of less than 2 bits per signal compared to ES.

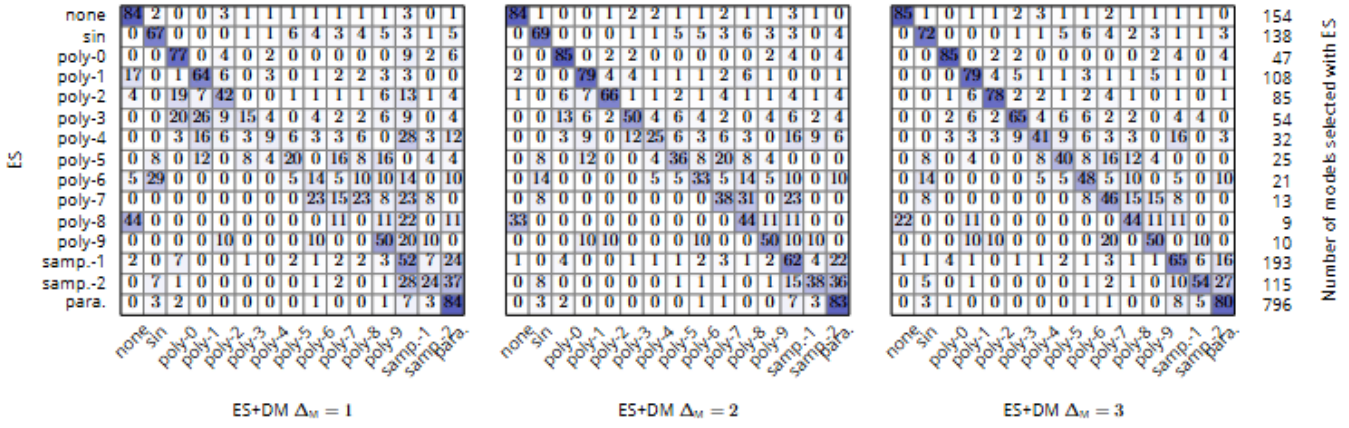


Fig. 12. Confusion matrices showing the percentage of model selection of the ES with DM compared to the ES approach when  $\Delta_M = 1$  (left),  $\Delta_M = 2$  (middle), and  $\Delta_M = 3$  (right). The number of selection of each model by the ES approach is on the right. Results are based on 1800 vectors of 128 samples from [84] with  $D_{\max} = 200^2 V^2$ .

Table II provides the average total bit rate obtained by the ES with DM to get a distortion below  $D_{\max} = 200 V^2$  for different values of  $\Delta_M$  and  $\Delta_{nx}$ , illustrating the compromise between compression efficiency and complexity. Considering  $\Delta_M = 3$  yields a significant complexity reduction with an increase of less than 10% of the required rate, whatever the value of  $\Delta_{nx}$ .

$\Delta_{nx}$ $\Delta_M$	1	3	5	7	9	33
1	101.7	97.2	95.6	94.6	94.2	92.6
2	98.2	94.2	93.0	92.4	91.9	90.4
3	96.7	93.4	91.9	91.4	90.9	89.5
14	94.3	91.7	90.1	89.5	89.16	87.9

TABLE II

AVERAGE TOTAL BIT RATE (BITS/WINDOW) ACHIEVED WITH THE ES WITH DM APPROACH CONSIDERING (32) WITH  $P_M = 1$  AND  $P_Q = 1$  FOR DIFFERENT VALUES OF  $\Delta_M$  AND  $\Delta_{nx}$ . RESULTS ARE AVERAGED ON 1800 VECTORS OF 128 SAMPLES FROM DIGITAL-FAULT-RECORDED DATABASE [84] WITH  $D_{\max} = 200^2 V^2$ .

#### D. Comparison with alternative approaches

The proposed approaches are compared to reference methods. The first has been proposed in [85] and involves a DWT followed by the EZW entropy coder <sup>2</sup>. The second is the technique from [85], which is based on a sparse representation using Overcomplete Hybrid Dictionaries (OHD) <sup>3</sup>. The third is the compression method from [81], which employs Wavelet Spectral Quantization Models (WSQM) <sup>4</sup>. The WSQM approach considering both linear and exponential decay models for spectral shape, balancing efficiency and complexity.

In this section, we first evaluate the impact of  $D_{\max}$  and of the window size  $N$  on the bitrate and on the compression efficiency. Then their impact on the computational cost is evaluated.

Figure 13 shows that the proposed approaches (ES, ES with DM, GSS, and GSS with DM) achieve the best performance in terms of bitrate for different distortion constraints  $D_{\max}$ , outperforming the reference methods (WSQM, OHD, and EZW). The proposed methods perform quite similarly, even if ES provides the best results, followed by GSS, then ES with DM, and finally GSS with DM.

Figure 14 shows that the proposed compression methods, ES with DM and ES with GSS, are more efficient in terms of computational time compared to ES and GSS. The computation time is proportional to the number of transforms performed per window, which is detailed in Table III for each method. Compared to WSQM, the methods ES with DM and ES with GSS achieve similar computation times while providing significantly better compression performance. Moreover, their computational advantage over WSQM increases with the window size  $N$ . However, when compared to OHD and EZW, the proposed methods still require significantly more computation time. This additional cost is the trade-off for achieving better compression performance on average compared to existing approaches.

ES (Sec IV-C)	GSS (Sec IV-D)	ES with DM (Sec V-C)	GSS with DM (Sec V-C)	OHD	WSQM	EZW
$\approx 100O(N \log(N))$	$\approx 74O(N \log(N))$	$\approx 16O(N \log(N))$	$\approx 11O(N \log(N))$	$\approx 20O(N^2)$	$\approx O(N \log(N))$	$\approx O(N \log(N))$

TABLE III

COMPUTATIONAL COMPLEXITY FOR DIFFERENT METHODS. THESE VALUES WERE OBTAINED EXPERIMENTALLY UNDER A CONSTRAINT OF  $D_{\max} = 200^2 V^2$ . FOR ES WITH DM,  $\Delta_M = 3$  AND  $\Delta_{Nx} = 7$ . FOR OHD, THE COMPUTATIONAL COST IS DETERMINED BY THE AVERAGE NUMBER OF SELECTED VECTORS ( $\approx 10$  FOR  $D_{\max} = 200^2 V^2$ .) MULTIPLIED BY THE DICTIONARY SIZE ( $2N$ ) AND THE SIGNAL DIMENSION ( $N$ ).

Table III presents the computational complexity, expressed as the number of transforms applied, for each method. The results indicate that the proposed methods in this paper involve higher computational costs than those in the literature, primarily due to additional evaluations required for precise model selection and bit allocation. Although these methods incur a higher computational cost compared to reference methods, even when considering ES with DM or GSS, the compression performance is significantly improved. This increase in computational cost is the trade-off required to achieve superior performance.

<sup>2</sup>Code available at this link: <https://github.com/CorentinPresvots/MMC-with-Rate-Constraint>

<sup>3</sup>Code available at this link: <https://github.com/CorentinPresvots/OHD>

<sup>4</sup>Code available at this link: <https://github.com/CorentinPresvots/WSQM>

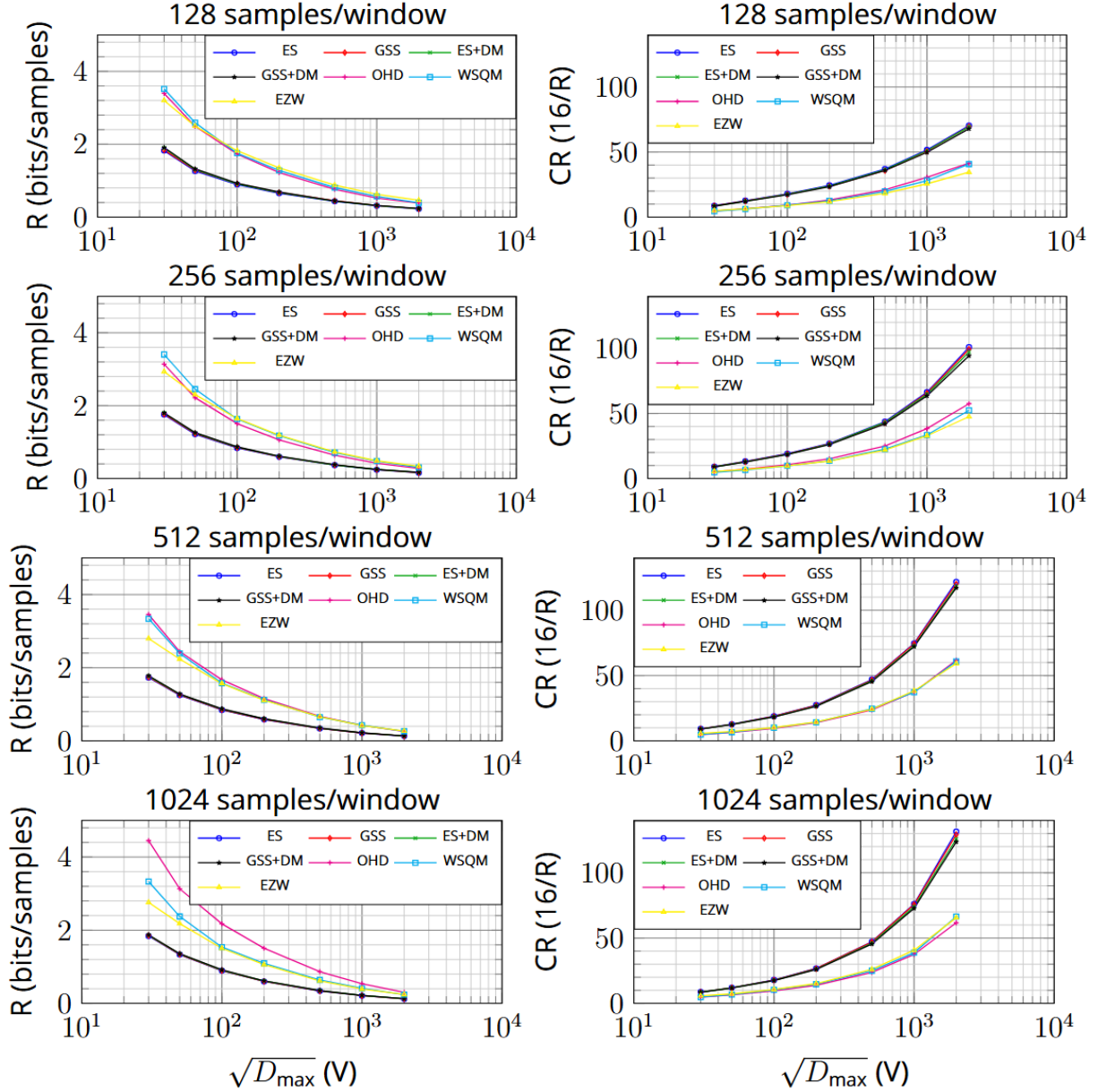


Fig. 13. Bitrate (left) and CR (right) as a function of  $\sqrt{D_{\max}}$  for ES, ES with DM, GSS, GSS with DM, WSQM, OHD, and EZW. Rows correspond to window sizes of 128, 256, 512, and 1024 samples, respectively. Results are averaged over the twelve first-phase voltage signals described in Section VI-A.

## VII. CONCLUSION

This paper considers the two-stage MMC scheme for VCS developed in [75] initially considering target rate constraints. The MMC scheme has been adapted to reach a target distortion constraint. Three approaches have been developed for selecting the signal model for the first stage and the optimal bit allocation between stages in order to satisfy a target distortion constraint while minimizing the required total rate. An ES serves as baseline. Using GSS, the rate selection is facilitated, but the approach may be suboptimal when the total rate required to meet the distortion target is not a convex function of the rate

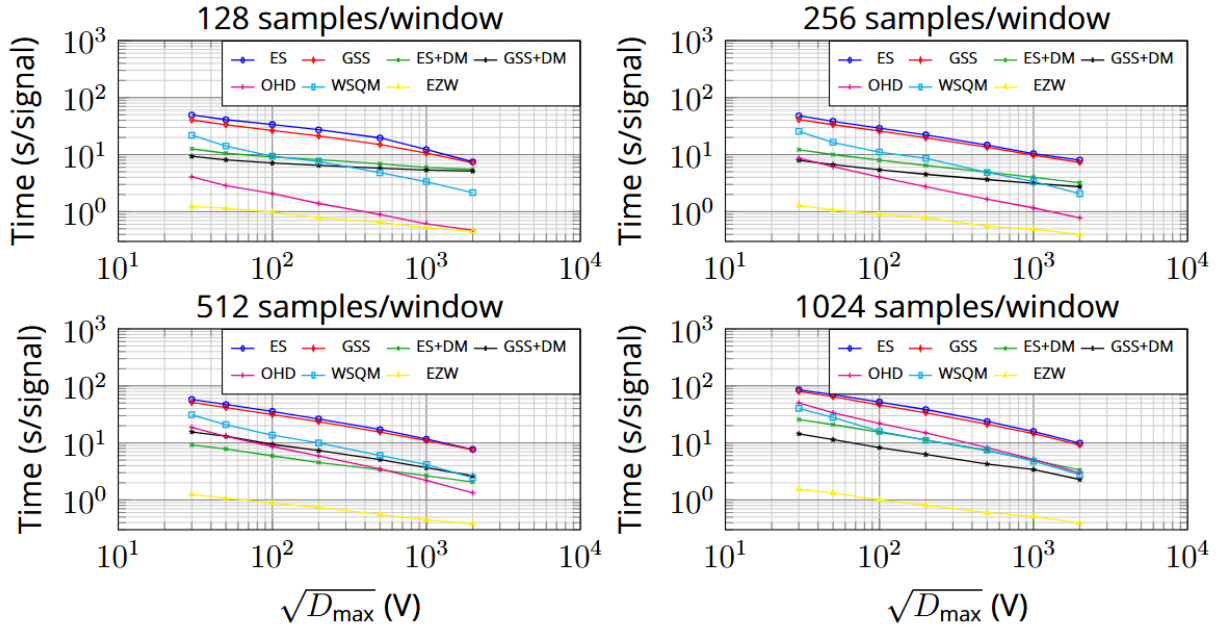


Fig. 14. Evolution of the average computation time required to encode each one-second signal duration using the proposed algorithms available at , for different  $D_{\max}$  constraints, considering ES, ES with DM, GSS, GSS with DM, WSQM, OHD, and EZW. The first row corresponds to window sizes of 128 and 256 samples, while the second row corresponds to 512 and 1024 samples, respectively. Results are averaged over the twelve first-phase voltage signals described in Section VI-A.

required for the first stage. The third method is based on a RD model of the total rate as a function of the rate of the first stage. A subset of promising candidate models can be selected and an approximate bit allocation for each of these models can be determined. They can then be fed to the two previous approaches to obtain refined estimates of the best signal model and rate allocation.

Experimental results confirm that the proposed methods outperform established techniques, such as OHD, WSQM, or EZW in terms of rate for a given distortion constraint. Furthermore, the reduced-complexity approaches (ES with DM and GSS) maintain performance close to the exhaustive search but at a fraction of the computational cost.

Future work will be dedicated to the exploitation of reinforcement learning techniques to select the best signal model in the first stage and the optimal bit allocation between stages accounting for the signal characteristics and the previously selected models.

## REFERENCES

- [1] Y. Gu and T. C. Green, "Power system stability with a high penetration of inverter-based resources," *Proceedings of the IEEE*, vol. 111, no. 7, pp. 832–853, 2023.
- [2] C. Presvôts, M. Kieffer, T. Prevost, P. Panciatici, Z. Li, and P. Piantanida, "Two-stage multiple-model compression approach for sampled electrical signals," in *Proc. IEEE Data Compression Conference*, 2024, pp. 522–531.
- [3] W. Ding and B. Liu, "Rate control of mpeg video coding and recording by rate-quantization modeling," *IEEE transactions on circuits and systems for video technology*, vol. 6, no. 1, pp. 12–20, 1996.

- [4] H. Choi, J. Yoo, J. Nam, D. Sim, and I. V. Bajić, “Pixel-wise unified rate-quantization model for multi-level rate control,” *IEEE Journal of Selected Topics in Signal Processing*, vol. 7, no. 6, pp. 1112–1123, 2013.
- [5] S. Ma, W. Gao, and Y. Lu, “Rate-distortion analysis for h. 264/avc video coding and its application to rate control,” *IEEE transactions on circuits and systems for video technology*, vol. 15, no. 12, pp. 1533–1544, 2005.
- [6] Y. Li, H. Jia, P. Ma, C. Zhu, X. Xie, and W. Gao, “Inter-dependent rate-distortion modeling for video coding and its application to rate control,” in *2014 IEEE International Conference on Multimedia and Expo (ICME)*. IEEE, 2014, pp. 1–6.
- [7] M. Aklouf, M. Leny, M. Kieffer, and F. Dufaux, “Interframe-dependent rate-qp-distortion model for video coding and transmission,” in *2021 IEEE International Conference on Image Processing (ICIP)*. IEEE, 2021, pp. 2019–2023.
- [8] M. Liu, Y. Guo, H. Li, and C. W. Chen, “Low-complexity rate control based on  $\rho$ -domain model for scalable video coding,” in *2010 IEEE International Conference on Image Processing*. IEEE, 2010, pp. 1277–1280.
- [9] M. Tang, J. Wen, and Y. Han, “A generalized rate-distortion- $\lambda$  model based hevc rate control algorithm,” *arXiv preprint arXiv:1911.00639*, 2019.
- [10] B. Li, H. Li, L. Li, and J. Zhang, “ $\lambda$  domain rate control algorithm for high efficiency video coding,” *IEEE transactions on Image Processing*, vol. 23, no. 9, pp. 3841–3854, 2014.
- [11] L. Li, B. Li, H. Li, and C. W. Chen, “ $\lambda$ -domain optimal bit allocation algorithm for high efficiency video coding,” *IEEE Transactions on Circuits and Systems for Video Technology*, vol. 28, no. 1, pp. 130–142, 2016.
- [12] X. Yang, Y. Tan, and N. Ling, “Rate control for h. 264 with two-step quantization parameter determination but single-pass encoding,” *EURASIP Journal on Advances in Signal Processing*, vol. 2006, no. 1, p. 063409, 2006.
- [13] L.-J. Lin and A. Ortega, “Bit-rate control using piecewise approximated rate-distortion characteristics,” *IEEE Transactions on Circuits and Systems for Video Technology*, vol. 8, no. 4, pp. 446–459, 1998.
- [14] X. M. Zhang, A. Vetro, Y. Q. Shi, and H. Sun, “Constant quality constrained rate allocation for fgs-coded video,” *IEEE Transactions on Circuits and Systems for Video Technology*, vol. 13, no. 2, pp. 121–130, 2003.
- [15] T. Huang, R.-X. Zhang, C. Zhou, and L. Sun, “Qarc: Video quality aware rate control for real-time video streaming based on deep reinforcement learning,” in *Proceedings of the 26th ACM international conference on Multimedia*, 2018, pp. 1208–1216.
- [16] M. Zhou, X. Wei, S. Kwong, W. Jia, and B. Fang, “Rate control method based on deep reinforcement learning for dynamic video sequences in hevc,” *IEEE Transactions on Multimedia*, vol. 23, pp. 1106–1121, 2020.
- [17] H. Schwarz, D. Marpe, and T. Wiegand, “Overview of the scalable video coding extension of the h. 264/avc standard,” *IEEE Transactions on circuits and systems for video technology*, vol. 17, no. 9, pp. 1103–1120, 2007.
- [18] J. M. Boyce, Y. Ye, J. Chen, and A. K. Ramasubramonian, “Overview of shvc: Scalable extensions of the high efficiency video coding standard,” *IEEE Transactions on Circuits and Systems for Video Technology*, vol. 26, no. 1, pp. 20–34, 2015.
- [19] T. Zhao, J. Wang, Z. Wang, and C. W. Chen, “Ssim-based coarse-grain scalable video coding,” *IEEE Transactions on Broadcasting*, vol. 61, no. 2, pp. 210–221, 2015.
- [20] R. Gupta, A. Pulipaka, P. Seeling, L. J. Karam, and M. Reisslein, “H. 264 coarse grain scalable (cgs) and medium grain scalable (mgs) encoded video: A trace based traffic and quality evaluation,” *IEEE Transactions on Broadcasting*, vol. 58, no. 3, pp. 428–439, 2012.
- [21] A. Skodras, C. Christopoulos, and T. Ebrahimi, “The jpeg 2000 still image compression standard,” *IEEE Signal processing magazine*, vol. 18, no. 5, pp. 36–58, 2001.
- [22] J. Shapiro, “Embedded image coding using zerotrees of wavelet coefficients,” *IEEE Transactions on Signal Processing*, vol. 41, no. 12, pp. 3445–3462, 1993.
- [23] D. Taubman and A. Zakhor, “Multirate 3-d subband coding of video,” *IEEE Transactions on image processing*, vol. 3, no. 5, pp. 572–588, 1994.
- [24] A. Said and W. A. Pearlman, “A new, fast, and efficient image codec based on set partitioning in hierarchical trees,” *IEEE Transactions on circuits and systems for video technology*, vol. 6, no. 3, pp. 243–250, 1996.
- [25] D. Taubman, “High performance scalable image compression with ebcot,” *IEEE Transactions on image processing*, vol. 9, no. 7, pp. 1158–1170, 2000.
- [26] M. Nguyen, H. Amirpour, C. Timmerer, and H. Hellwagner, “Scalable high efficiency video coding based http adaptive streaming over quic,” in *Proceedings of the Workshop on the Evolution, Performance, and Interoperability of QUIC*, 2020, pp. 28–34.

- [27] F. Kossentini, H. Guermazi, N. Mahdi, C. Nouira, A. Naghdinezhad, H. Tmar, O. Khelif, P. Worth, and F. B. Amara, “The svt-av1 encoder: overview, features and speed-quality tradeoffs,” in *Applications of Digital Image Processing XLIII*, vol. 11510. SPIE, 2020, pp. 469–490.
- [28] S. Battista, G. Meardi, S. Ferrara, L. Ciccarelli, F. Maurer, M. Conti, and S. Orcioni, “Overview of the low complexity enhancement video coding (lcevc) standard,” *IEEE Transactions on Circuits and Systems for Video Technology*, vol. 32, no. 11, pp. 7983–7995, 2022.
- [29] J. Ballé, V. Laparra, and E. P. Simoncelli, “End-to-end optimized image compression,” *arXiv preprint arXiv:1611.01704*, 2016.
- [30] J. Ballé, D. Minnen, S. Singh, S. J. Hwang, and N. Johnston, “Variational image compression with a scale hyperprior,” *arXiv preprint arXiv:1802.01436*, 2018.
- [31] J. Lee, S. Cho, and S.-K. Beack, “Context-adaptive entropy model for end-to-end optimized image compression,” *arXiv preprint arXiv:1809.10452*, 2018.
- [32] F. Kong, G. Ren, Y. Hu, D. Li, and K. Hu, “Mixture autoregressive and spectral attention network for multispectral image compression based on variational autoencoder,” *The Visual Computer*, pp. 1–24, 2023.
- [33] C. C. Aggarwal, *Neural Networks and Deep Learning: A Textbook*. Springer, 2023.
- [34] Y. Mei, L. Li, Z. Li, and F. Li, “Learning-based scalable image compression with latent-feature reuse and prediction,” *IEEE Transactions on Multimedia*, vol. 24, pp. 4143–4157, 2021.
- [35] D. Zhang, F. Li, M. Liu, R. Cong, H. Bai, M. Wang, and Y. Zhao, “Exploring resolution fields for scalable image compression with uncertainty guidance,” *IEEE Transactions on Circuits and Systems for Video Technology*, 2023.
- [36] H. Fu, F. Liang, J. Liang, Z. Fang, G. Zhang, and J. Han, “Learned image compression with dual-branch encoder and conditional information coding,” in *2024 Data Compression Conference (DCC)*. IEEE, 2024, pp. 173–182.
- [37] S. Santoso, E. J. Powers, and W. M. Grady, “Power quality disturbance data compression using wavelet transform methods,” *IEEE Transactions on Power Delivery*, vol. 12, no. 3, pp. 1250–1257, 1997.
- [38] J. Chung, E. J. Powers, W. M. Grady, and S. C. Bhatt, “Electric power transient disturbance classification using wavelet-based hidden markov models,” in *International Conference on Acoustics, Speech, and Signal Processing*, vol. 6. IEEE, 2000, pp. 3662–3665.
- [39] I. Y.-H. Gu and E. Styvaktakis, “Bridge the gap: signal processing for power quality applications,” *Elsevier Electric Power Systems Research*, vol. 66, no. 1, pp. 83–96, 2003.
- [40] M. V. Ribeiro and J. L. R. Pereira, “Classification of single and multiple disturbances in electric signals,” *EURASIP Journal on Advances in Signal Processing*, vol. 2007, pp. 1–18, 2007.
- [41] M. H. Bollen, I. Y. Gu, S. Santoso, M. F. McGranaghan, P. A. Crossley, M. V. Ribeiro, and P. F. Ribeiro, “Bridging the gap between signal and power,” *IEEE Signal processing magazine*, vol. 26, no. 4, pp. 12–31, 2009.
- [42] S. Khokhar, A. A. M. Zin, A. P. Memon, and A. S. Mokhtar, “A new optimal feature selection algorithm for classification of power quality disturbances using discrete wavelet transform and probabilistic neural network,” *Elsevier Measurement*, vol. 95, pp. 246–259, 2017.
- [43] Y. Yan, K. Chen, H. Geng, W. Fan, and X. Zhou, “A review on intelligent detection and classification of power quality disturbances: Trends, methodologies, and prospects,” *Computer Modeling in Engineering and Sciences*, vol. 137, no. 2, pp. 1345–1379, 2023.
- [44] IEEE, *Standard for Synchrophasor Data Transfer for Power Systems*, Std. Std C37.118.2-2011, 2011.
- [45] R. Klump, P. Agarwal, J. E. Tate, and H. Khurana, “Lossless compression of synchronized phasor measurements,” in *Power Engineering SocietyGeneral Meeting*. IEEE, 2010, pp. 1–7.
- [46] M. Paolone, T. Gaunt, X. Guillaud, M. Liserre, S. Meliopoulos, A. Monti, T. Van Cutsem, V. Vittal, and C. Vournas, “Fundamentals of power systems modelling in the presence of converter-interfaced generation,” *Electric Power Systems Research*, vol. 189, p. 106811, 2020.
- [47] J. Zygarlicki and J. Mroczka, “Data compression using prony’s method and wavelet transform in power quality monitoring systems,” *PAN Metrology and Measurement Systems*, vol. 13, no. 3, pp. 325–251, 2006.
- [48] J. Zygarlicki, M. Zygarlicka, J. Mroczka, and K. J. Latawiec, “A reduced prony’s method in power-quality analysis-parameters selection,” *IEEE Transactions on Power Delivery*, vol. 25, no. 2, pp. 979–986, 2010.
- [49] L. Lovisolo, E. da Silva, M. Rodrigues, and P. Diniz, “Efficient coherent adaptive representations of monitored electric signals in power systems using damped sinusoids,” *IEEE Trans. Signal Processing*, vol. 53, no. 10, pp. 3831–3846, 2005.

[50] L. Lovisolo, M. P. Tcheou, E. A. da Silva, M. A. Rodrigues, and P. S. Diniz, "Modeling of electric disturbance signals using damped sinusoids via atomic decompositions and its applications," *EURASIP Journal on Advances in Signal Processing*, vol. 2007, pp. 1–15, 2007.

[51] M. P. Tcheou, L. Lovisolo, E. A. B. da Silva, M. A. M. Rodrigues, and P. S. R. Diniz, "Optimum rate-distortion dictionary selection for compression of atomic decompositions of electric disturbance signals," *IEEE Signal Processing Letters*, vol. 14, no. 2, pp. 81–84, 2007.

[52] M. P. Tcheou, A. L. Miranda, L. Lovisolo, E. A. da Silva, M. A. Rodrigues, and P. S. Diniz, "How far can one compress digital fault records? analysis of a matching pursuit-based algorithm," *Elsevier Digital Signal Processing*, vol. 22, no. 2, pp. 288–297, 2012.

[53] A. Karpilow, A. Derviškadić, G. Frigo, and M. Paolone, "Characterization of non-stationary signals in electric grids: A functional dictionary approach," *IEEE Transactions on Power Systems*, vol. 37, no. 2, pp. 1126–1138, 2021.

[54] A. C. Karpilow, "Functional-basis analysis of non-stationary signals in modern power grids: Theory and implementation in embedded systems," EPFL, Tech. Rep., 2024.

[55] M. Yaghoobi, L. Daudet, and M. E. Davies, "Parametric dictionary design for sparse coding," *IEEE Transactions on Signal Processing*, vol. 57, no. 12, pp. 4800–4810, 2009.

[56] F. A. de Oliveira Nascimento, "Data compression algorithm for transient recording system," in *International Symposium on Industrial Electronics*. IEEE, 1997, pp. 1126–1130.

[57] A. Qing, Z. Hongtao, H. Zhikun, and C. Zhiwen, "A compression approach of power quality monitoring data based on two-dimension DCT," in *Proc. IEEE Int. Conf. Measuring Technology and Mechatronics Automation*, vol. 1, 2011, pp. 20–24.

[58] R. E. Dapper, A. A. Susin, S. Bampi, and C. D. P. Crovato, "High compression ratio algorithm for power quality signals," in *International Symposium on Industrial Electronics*. IEEE, 2015, pp. 1322–1326.

[59] E. B. Kapisch, V. V. de Moraes, L. R. M. Silva, L. M. A. Filho, and C. A. Duque, "Spectral variation-based signal compression technique for gapless power quality waveform recording in smart grids," *IEEE Transactions on Industrial Informatics*, vol. 18, no. 7, pp. 4488–4498, 2022.

[60] T. Littler and D. Morrow, "Wavelets for the analysis and compression of power system disturbances," *IEEE Transactions on Power Delivery*, vol. 14, no. 2, pp. 358–364, 1999.

[61] J. Chung, E. Powers, W. Grady, and S. Bhatt, "Variable rate power disturbance signal compression using embedded zerotree wavelet transform coding," in *Power Engineering Society*, vol. 2. IEEE, 1999, pp. 1305–1309 vol.2.

[62] C.-T. Hsieh and S.-J. Huang, "Disturbance data compression of a power system using the huffman coding approach with wavelet transform enhancement," *IET Proceedings: Generation, Transmission and Distribution*, vol. 150, no. 1, pp. 7–14, 2003.

[63] C.-J. Wu, T.-H. Fu, and C.-P. Huang, "Data compression technique in recording electric arc furnace voltage and current waveforms for tracking power quality," in *Proc. IEEE Transmission and Distribution Conference and Exposition*, vol. 1. IEEE, 2003, pp. 383–388.

[64] L. Shang, J. Jaeger, and R. Krebs, "Efficiency analysis of data compression of power system transients using wavelet transform," in *Bologna Power Tech Conference Proceedings*, vol. 4. IEEE, 2003, pp. 6–pp.

[65] Y. Yuan, X. Yu, and H. Du, "Power system fault data compression using the wavelet transform and vector quantification," in *International Conference on Power System Technology*. IEEE, 2006, pp. 1–6.

[66] J. Ning, J. Wang, W. Gao, and C. Liu, "A wavelet-based data compression technique for smart grid," *IEEE Transactions on Smart Grid*, vol. 2, no. 1, pp. 212–218, 2011.

[67] E. Prathibha, A. Manjunatha, and S. Basavaraj, "Dual tree complex wavelet transform based approach for power quality monitoring and data compression," in *Biennial International Conference on Power and Energy Systems: Towards Sustainable Energy*. IEEE, 2016, pp. 1–5.

[68] G. Panda, P. Dash, A. K. Pradhan, and S. K. Meher, "Data compression of power quality events using the slantlet transform," *IEEE Transactions on power delivery*, vol. 17, no. 2, pp. 662–667, 2002.

[69] P. Dash, B. Panigrahi, D. Sahoo, and G. Panda, "Power quality disturbance data compression, detection, and classification using integrated spline wavelet and s-transform," *IEEE Transactions on Power Delivery*, vol. 18, no. 2, pp. 595–600, 2003.

[70] S. K. Meher, A. Pradhan, and G. Panda, "An integrated data compression scheme for power quality events using spline wavelet and neural network," *Elsevier Electric Power Systems Research*, vol. 69, no. 2–3, pp. 213–220, 2004.

[71] S.-J. Huang and M.-J. Jou, "Application of arithmetic coding for electric power disturbance data compression with wavelet packet enhancement," *IEEE Transactions on Power Systems*, vol. 19, no. 3, pp. 1334–1341, 2004.

[72] F. Lorio and F. Magnago, "Analysis of data compression methods for power quality events," in *Power Engineering Society General Meeting*, vol. 1. IEEE, 2004, pp. 504–509.

[73] F. A. de Oliveira Nascimento, "Hartley transform signal compression and fast power quality measurements for smart grid application," *IEEE Transactions on Power Delivery*, 2023.

[74] X. Wang, Y. Liu, and L. Tong, "Adaptive subband compression for streaming of continuous point-on-wave and PMU data," *IEEE Transactions on Power Systems*, vol. 36, no. 6, pp. 5612–5621, 2021.

[75] C. Presvôts, M. Kieffer, T. Prevost, P. Panciatici, L. Zuxing, and P. Piantanida, "Multiple-model coding scheme for electrical signal compression," *Signal Processing*, vol. 236, 2025.

[76] E. Hamid and Z.-I. Kawasaki, "Wavelet-based data compression of power system disturbances using the minimum description length criterion," *IEEE Transactions on Power Delivery*, vol. 17, no. 2, pp. 460–466, 2002.

[77] Y. Linde, A. Buzo, and R. Gray, "An algorithm for vector quantizer design," *IEEE Transactions on communications*, vol. 28, no. 1, pp. 84–95, 1980.

[78] J. Rissanen, "Modeling by shortest data description," *Elsevier Automatica*, vol. 14, no. 5, pp. 465–471, 1978.

[79] J. Khan, "Weighted entropy and modified mdl for compression and denoising data in smart grid," *Elsevier International Journal of Electrical Power & Energy Systems*, vol. 133, p. 107089, 2021.

[80] J. Cormane and F. A. de O. Nascimento, "Spectral shape estimation in data compression for smart grid monitoring," *IEEE Transactions on Smart Grid*, vol. 7, no. 3, pp. 1214–1221, 2016.

[81] F. A. d. O. Nascimento, R. G. Saraiva, and J. Cormane, "Improved transient data compression algorithm based on wavelet spectral quantization models," *IEEE Transactions on Power Delivery*, vol. 35, no. 5, pp. 2222–2232, 2020.

[82] J. Khan, S. M. A. Bhuiyan, G. Murphy, and M. Arline, "Embedded-zerotree-wavelet-based data denoising and compression for smart grid," *IEEE Transactions on Industry Applications*, vol. 51, no. 5, pp. 4190–4200, 2015.

[83] T. M. N. Hoang, S. Ragot, M. Oger, and M. Antonini, "A new bitplane coder for scalable transform audio coding," in *International Conference on Acoustics, Speech and Signal Processing*. IEEE, 2009, pp. 4137–4140.

[84] C. Presvôts and T. Prevost. (2024) Database of voltage and current samples values from the french electricity transmission grid, rÃ©seau de transport d'electricitÃ© (RTE), france. [Online]. Available: <https://github.com/rte-france/digital-fault-recording-database>

[85] M. Sabarimalai Manikandan, S. R. Samantaray, and I. Kamwa, "Simultaneous denoising and compression of power system disturbances using sparse representation on overcomplete hybrid dictionaries," *Wiley Online Library IET Generation, Transmission & Distribution*, vol. 9, no. 11, pp. 1077–1088, 2015.

[86] S. He, W. Tian, J. Zhang, K. Li, M. Zhang, and R. Zhu, "A high efficient approach for power disturbance waveform compression in the view of heisenberg uncertainty," *IEEE Transactions on Industrial Informatics*, vol. 15, no. 5, pp. 2580–2591, 2019.

[87] G. A. de Oliveira, M. P. Tcheou, and L. Lovisolo, "Artificial neural networks for dictionary selection in adaptive greedy decomposition algorithms with reduced complexity," in *International Joint Conference on Neural Networks*. IEEE, 2018, pp. 1–8.

[88] M. Ruiz and I. Montalvo, "Electrical faults signals restoring based on compressed sensing techniques," *MDPI Energies*, vol. 13, no. 8, p. 2121, 2020.

[89] S. G. Mallat and Z. Zhang, "Matching pursuits with time-frequency dictionaries," *IEEE Transactions on signal processing*, vol. 41, no. 12, pp. 3397–3415, 1993.

[90] M. V. Ribeiro, S. H. Park, J. M. T. Romano, and S. K. Mitra, "A novel mdl-based compression method for power quality applications," *IEEE Transactions on Power Delivery*, vol. 22, no. 1, pp. 27–36, 2007.

[91] M. Zhang, K. Li, and Y. Hu, "A high efficient compression method for power quality applications," *IEEE Transactions on Instrumentation and Measurement*, vol. 60, no. 6, pp. 1976–1985, 2011.

[92] N. C. F. Tse, J. Y. C. Chan, W.-H. Lau, J. T. Y. Poon, and L. L. Lai, "Real-time power-quality monitoring with hybrid sinusoidal and lifting wavelet compression algorithm," *IEEE Transactions on Power Delivery*, vol. 27, no. 4, pp. 1718–1726, 2012.

[93] W. Hao, B. Hu, and L. Zhao, "Compression of power quality disturbance using wavelet-atomic decomposition for grid-connected wind farms," in *Proc. IEEE Int. Conf. Electrical Engineering and Green Energy*, 2023, pp. 171–178.

[94] U. Kamps, “Chebyshev polynomials and least squares estimation based on one-dependent random variables,” *Elsevier Linear Algebra and its Applications*, vol. 112, pp. 217–230, 1989.

[95] V. Alves de Oliveira, M. Chabert, T. Oberlin, C. Poulliat, M. Bruno, C. Latry, M. Caravan, S. Henrot, F. Falzon, and R. Camarero, “Reduced-complexity end-to-end variational autoencoder for on board satellite image compression,” *Remote Sensing*, vol. 13, no. 3, p. 447, 2021.

[96] P. Panter and W. Dite, “Quantization distortion in pulse-count modulation with nonuniform spacing of levels,” *Proceedings of the IRE*, vol. 39, no. 1, pp. 44–48, 1951.

[97] K. Sayood, *Introduction to Data Compression*, 5th ed. San Francisco, CA: Morgan Kaufmann, 2017.

[98] W. H. Press, S. A. Teukolsky, W. T. Vetterling, and B. P. Flannery, *Golden Section Search in One Dimension*. Cambridge University Press, ch. 10.2.

[99] T. M. Cover, *Elements of information theory*. John Wiley & Sons, 1999.

[100] G. T. Walker, “On periodicity in series of related terms,” in *Series A, Containing Papers of a Mathematical and Physical Character*, vol. 131, no. 818. The Royal Society London, 1931, pp. 518–532.

[101] CEI IEC, *60044-1:2003 International Standard Instrument Transformers*, Std., 2003.

## APPENDIX

### A. Proof of Propositions 1 and 3

The first-order Taylor expansion of  $\mathbf{x}^m(\hat{\boldsymbol{\theta}})$  at  $\hat{\boldsymbol{\theta}}_q(n_x)$  is

$$\mathbf{x}^m(\hat{\boldsymbol{\theta}}) \simeq \mathbf{x}^m(\hat{\boldsymbol{\theta}}_q(n_x)) + \frac{\partial \mathbf{x}^m(\hat{\boldsymbol{\theta}})}{\partial \hat{\boldsymbol{\theta}}^T} \boldsymbol{\varepsilon}(\hat{\boldsymbol{\theta}}, n_x), \quad (48)$$

where  $\boldsymbol{\varepsilon}(\hat{\boldsymbol{\theta}}, n_x) = \hat{\boldsymbol{\theta}} - \hat{\boldsymbol{\theta}}_q(n_x)$ . Consequently,

$$\mathbf{e}_q^m(\hat{\boldsymbol{\theta}}, n_x) = \frac{\partial \mathbf{x}^m(\hat{\boldsymbol{\theta}})}{\partial \hat{\boldsymbol{\theta}}^T} \boldsymbol{\varepsilon}(\hat{\boldsymbol{\theta}}, n_x). \quad (49)$$

The biased estimate of the autocorrelation function of  $\mathbf{e}_q^m(\hat{\boldsymbol{\theta}}, n_x)$  is

$$\hat{\gamma}_q^m(p, \hat{\boldsymbol{\theta}}, n_x) = \frac{1}{N} \sum_{n=p+1}^N e_{q,n}^m(\hat{\boldsymbol{\theta}}, n_x) e_{q,n-p}^m(\hat{\boldsymbol{\theta}}, n_x) \quad (50)$$

$$= \frac{1}{N} \text{Tr} \left( \begin{pmatrix} \frac{\partial x_{p+1}^m(\hat{\boldsymbol{\theta}})}{\partial \hat{\theta}_1} & \dots & \frac{\partial x_{p+1}^m(\hat{\boldsymbol{\theta}})}{\partial \hat{\theta}_K} \\ \vdots & \ddots & \vdots \\ \frac{\partial x_N^m(\hat{\boldsymbol{\theta}})}{\partial \hat{\theta}_1} & \dots & \frac{\partial x_N^m(\hat{\boldsymbol{\theta}})}{\partial \hat{\theta}_K} \end{pmatrix} \begin{pmatrix} \varepsilon_1^2 & \dots & \varepsilon_1 \varepsilon_K \\ \vdots & \ddots & \vdots \\ \varepsilon_K \varepsilon_1 & \dots & \varepsilon_K^2 \end{pmatrix} \begin{pmatrix} \frac{\partial x_1^m(\hat{\boldsymbol{\theta}})}{\partial \hat{\theta}_1} & \dots & \frac{\partial x_{N-p}^m(\hat{\boldsymbol{\theta}})}{\partial \hat{\theta}_1} \\ \vdots & \ddots & \vdots \\ \frac{\partial x_1^m(\hat{\boldsymbol{\theta}})}{\partial \hat{\theta}_K} & \dots & \frac{\partial x_{N-p}^m(\hat{\boldsymbol{\theta}})}{\partial \hat{\theta}_K} \end{pmatrix} \right) \quad (51)$$

$$= \frac{1}{N} \text{Tr} \left( \begin{pmatrix} \sum_{k=1}^K \sum_{\ell=1}^K \varepsilon_k \varepsilon_{\ell} \frac{\partial x_{p+1}^m(\hat{\boldsymbol{\theta}})}{\partial \hat{\theta}_k} \frac{\partial x_1^m(\hat{\boldsymbol{\theta}})}{\partial \hat{\theta}_{\ell}} & \dots & * \\ \vdots & \ddots & \vdots \\ * & \dots & \sum_{k=1}^K \sum_{\ell=1}^K \varepsilon_k \varepsilon_{\ell} \frac{\partial x_N^m(\hat{\boldsymbol{\theta}})}{\partial \hat{\theta}_k} \frac{\partial x_{N-p}^m(\hat{\boldsymbol{\theta}})}{\partial \hat{\theta}_{\ell}} \end{pmatrix} \right). \quad (52)$$

Taking the expectation with respect to  $\boldsymbol{\varepsilon}(\hat{\boldsymbol{\theta}}, n_x)$ , one obtains

$$\mathbb{E}_{\boldsymbol{\varepsilon}} \left[ \hat{\gamma}_q^m(p, \hat{\boldsymbol{\theta}}, n_x) \right] = \mathbb{E}_{\boldsymbol{\varepsilon}} \left[ \frac{1}{N} \sum_{n=p+1}^N \sum_{k=1}^K \sum_{\ell=1}^K \varepsilon_k \varepsilon_{\ell} \frac{\partial x_n^m(\hat{\boldsymbol{\theta}})}{\partial \hat{\theta}_k} \frac{\partial x_{n-p}^m(\hat{\boldsymbol{\theta}})}{\partial \hat{\theta}_{\ell}} \right]. \quad (53)$$

The components  $\varepsilon_k(\hat{\boldsymbol{\theta}}, n_x)$  of  $\boldsymbol{\varepsilon}(\hat{\boldsymbol{\theta}}, n_x)$  are assumed zero-mean and uncorrelated for all  $k = 1, \dots, K$ . Consequently

$$\hat{\gamma}_q^m(p, \hat{\boldsymbol{\theta}}, n_x) = \mathbb{E}_{\boldsymbol{\varepsilon}} \left[ \hat{\gamma}_q^m(p, \hat{\boldsymbol{\theta}}, n_x) \right] \quad (54)$$

$$= \sum_{k=1}^K h_k(p, \hat{\boldsymbol{\theta}}) \mathbb{E}_{\boldsymbol{\varepsilon}} \left( \varepsilon_k^2(\hat{\boldsymbol{\theta}}, n_x) \right), \quad (55)$$

with

$$h_k(p, \hat{\boldsymbol{\theta}}) = \frac{1}{N} \sum_{n=p+1}^N \frac{\partial x_n^m(\hat{\boldsymbol{\theta}})}{\partial \hat{\theta}_k} \frac{\partial x_{n-p}^m(\hat{\boldsymbol{\theta}})}{\partial \hat{\theta}_k}. \quad (56)$$

The result of Proposition 1 is obtained taking  $p = 0$  in (56).

### B. Auto-correlation function for sinusoidal model

Consider the sinusoidal model with a single sinusoidal component (2) with estimated parameters  $\hat{\boldsymbol{\theta}} = (\hat{a}, \hat{f}, \hat{\phi})$ . Using Proposition 3, one has to evaluate

$$\frac{\partial x_n^m(\hat{\boldsymbol{\theta}})}{\partial \hat{a}} = \cos(2\pi \hat{f} n T_s + \hat{\phi}),$$

which leads to

$$\begin{aligned} h_1(p, \hat{\boldsymbol{\theta}}) &= \frac{1}{N} \sum_{n=p+1}^N \cos(2\pi \hat{f} n T_s + \hat{\phi}) \cos(2\pi \hat{f} (n-p) T_s + \hat{\phi}) \\ &= \frac{1}{2N} \sum_{n=p+1}^N \left( \cos(2\pi \hat{f} (2n-p) T_s + 2\hat{\phi}) + \cos(2\pi \hat{f} p T_s) \right). \end{aligned}$$

Then

$$\begin{aligned} \sum_{n=p+1}^N \cos(2\pi \hat{f} (2n-p) T_s + 2\hat{\phi}) &= \Re \left( \sum_{n=p+1}^N e^{2j\pi \hat{f} (2n-p) T_s + 2j\hat{\phi}} \right) \\ &= \cos(2\pi \hat{f} (N+1) T_s + 2\hat{\phi}) \frac{\sin(2\pi \hat{f} (N-p) T_s)}{\sin(2\pi \hat{f} T_s)}, \end{aligned}$$

after some basic calculus, where  $\Re(z)$  is the real part of  $z \in \mathbb{C}$ . Finally,

$$h_1(p, \hat{\boldsymbol{\theta}}) = \frac{1}{2N} \left( \cos(2\pi \hat{f} (N+1) T_s + 2\hat{\phi}) \frac{\sin(2\pi \hat{f} (N-p) T_s)}{\sin(2\pi \hat{f} T_s)} + (N-p) \cos(2\pi \hat{f} p T_s) \right).$$

One has also to evaluate

$$\frac{\partial x_n^m(\hat{\boldsymbol{\theta}})}{\partial \hat{f}} = -2\pi n T_s \sin(2\pi \hat{f} n T_s + \hat{\phi}),$$

to get

$$h_2(p, \hat{\theta}) = \frac{1}{N} \sum_{n=p+1}^N 4\pi^2 n(n-p) T_s^2 \hat{a}^2 \sin(2\pi \hat{f} n T_s + \hat{\phi}) \sin(2\pi \hat{f} (n-p) T_s + \hat{\phi})$$

for which a more compact expression is difficult to get.

Finally,

$$\frac{\partial x_n^m(\hat{\theta})}{\partial \hat{\phi}} = -\hat{a} \sin(2\pi \hat{f} n T_s + \hat{\phi})$$

leads to

$$\begin{aligned} h_3(p, \hat{\theta}) &= \frac{1}{N} \sum_{n=p+1}^N \hat{a}^2 \sin(2\pi \hat{f} n T_s + \hat{\phi}) \sin(2\pi \hat{f} (n-p) T_s + \hat{\phi}) \\ &= \frac{\hat{a}^2}{2N} \left( -\cos(2\pi \hat{f} (N+1) T_s + 2\hat{\phi}) \frac{\sin(2\pi \hat{f} (N-p) T_s)}{\sin(2\pi \hat{f} T_s)} + (N-p) \cos(2\pi \hat{f} p T_s) \right), \end{aligned}$$

obtained via the same derivation as those used to obtain  $h_1(p, \hat{\theta})$ .

### C. Auto-correlation function for polynomial model

Consider the Tchebychev polynomial model of degree  $K-1$  with estimated parameters  $\hat{\theta}_k$ ,  $k = 1, \dots, K$  given by (3). Using Proposition 3, one has to evaluate

$$\frac{\partial x_n^m(\hat{\theta})}{\partial \hat{\theta}_k} = \mathcal{T}_{k-1}\left(2\frac{n}{N} - 1\right)$$

to get

$$h_k^m(p) = \frac{1}{N} \sum_{n=p+1}^N \mathcal{T}_{k-1}\left(2\frac{n}{N} - 1\right) \mathcal{T}_{k-1}\left(2\frac{n-p}{N} - 1\right),$$

independent of  $\hat{\theta}$ .

### D. Auto-correlation function for sample predictive model

Consider the sample predictive coding approach of order  $K$ , offset  $\eta$ , and estimated parameters  $\hat{\theta}_k$ ,  $k = 1, \dots, K$  given by (4). Using Proposition 3, one has to evaluate

$$\frac{\partial x_n^m(\hat{\theta})}{\partial \hat{\theta}_k} = \hat{x}_{(i-1)N+n-\eta-k+1}$$

to get

$$h_k(p) = \frac{1}{N} \sum_{n=p+1}^N \hat{x}_{(i-1)N+n-\eta-k+1} \hat{x}_{(i-1)N+n-p-\eta-k+1},$$

independent of  $\hat{\theta}$ .